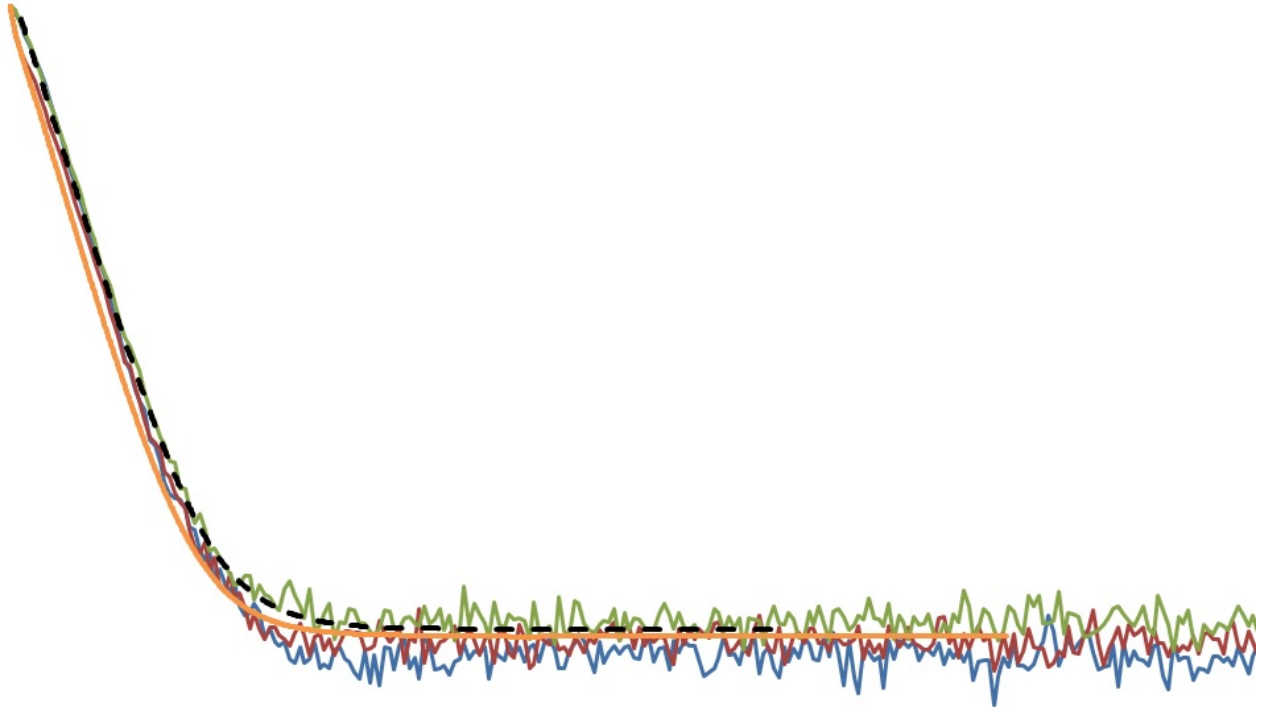




CHALMERS



Application of Deterministic Codes for Transient Analyses in Accelerator Driven Systems

A thesis presented by **Jessica Lybark** for the degree of master of science in Nuclear Science and Technology

DEPARTMENT OF PHYSICS
CHALMERS UNIVERSITY OF TECHNOLOGY
Gothenburg, Sweden, 2017
Master thesis TIFX05
Serial number CTH-NT-329
ISSN 1653-4662

Thesis for the Master of Science Degree
**Application of Deterministic Codes
for Transient Analyses in Accelerator
Driven Systems**



CHALMERS
UNIVERSITY OF TECHNOLOGY

SUPERVISOR: DR.-ING. FABRIZIO GABRIELLI
KARLSRUHE INSTITUTE OF TECHNOLOGY
KARLSRUHE, GERMANY

EXAMINERS: ASSOC. PROF. PAOLO VINAI
CHALMERS UNIVERSITY OF TECHNOLOGY
GOTHENBURG, SWEDEN

JESSICA LYBARK
DEPARTMENT OF PHYSICS
CHALMERS UNIVERSITY OF TECHNOLOGY
GOTHENBURG, SWEDEN, 2017

**Application of Deterministic Codes for Transient Analyses in
Accelerator Driven Systems**
JESSICA LYBARK

©Jessica Lybark, 2017

MASTER THESIS TIFX05
SERIAL NUMBER CTH-NT-329
ISSN 1653-4662
DEPARTMENT OF PHYSICS
CHALMERS UNIVERSITY OF TECHNOLOGY
GOTHENBURG
SWEDEN, 2017

The research was performed at
KARLSRUHE INSTITUTE OF TECHNOLOGY (KIT)
INSTITUTE FOR NUCLEAR AND ENERGY TECHNOLOGIES (IKET)
HERMANN-VON-HELMHOLTZ-PLATZ 1
76344 EGGENSTEIN-LEOPOLDSHAFEN
GERMANY



Abstract

Accelerator Driven Systems (ADSs) have been studying since long as a promising option for waste transmutation and energy production. In ADS the use of an external source causes the flux profiles to be different from the fundamental mode which characterize the critical reactors. These spatial effects are of interest to analyse for improving the accuracy and reliability of nuclear data and codes. In particular, validation of the kinetics models employed by the deterministic codes which are embedded in the safety codes is of great importance.

The aim of the thesis is to analyse the capabilities of the deterministic codes to predict the static and time-dependent detector responses from an external neutron pulse of two core configurations at different subcritical levels of Kyoto University Critical Assembly (KUCA), located at the Kyoto University Research Reactor Institute (KURRI). The aim was also to predict the experimental results of the application of the Pulsed Neutron Source (PNS) area method for reactivity inferring. The current work is performed in the framework of the participation of KIT to the calculation benchmark launched by the KURRI, on the analysis of the Phase-I kinetics experiments performed at KUCA. This is done in the frame of the IAEA Collaborative work on 'Accelerator Driven Systems (ADS) and Use of Low-Enriched Uranium (LEU) in ADS'. A 3D (XYZ) model of KUCA configurations and self-shielded multigroup cross sections were processed by means of the European Cell Code (ECCO). The 3D transport calculation has been performed by means of the European Reactor ANalysis Optimized System (ERANOS) and PARallel TIME-dependent SN code (PARTISN). The simulation results were compared with the reference experimental data in means of criticality level and kinetic parameters. Furthermore, were the codes employed to analyse the experimental results coming from the application of PNS area method.

Transient simulations were performed with KIN3D/VARIANT and KIN3D/PARTISN deterministic codes, with the purpose of analysing the time-dependent detector responses to an external neutron pulse. Calculation results show a good agreement with the kinetic experiments from KUCA. In particular, were the codes able to reproduce the reference PNS results and the experimental transient.

Keywords: ADS, reactivity, ERANOS, ECCO, KIN3D, VARIANT, PARTISN, PNS area method

Acknowledgements

I would first like to thank my thesis supervisors Dr. Fabrizio Gabrielli at Karlsruhe Institute of Technology (KIT) and Prof. Paolo Vinai at Chalmers University of Technology for guidance and fantastic support. I would like to extend my thanks to you both for the opportunity to do my master thesis at KIT, and the support during the thesis and the finishing of the report. It has been an inspiring time and I'm grateful that I been presented with a very interesting topic.

I would like to extend a special thanks to Fabrizio, this thesis would not have been the same without your never-ending support! Thanks for all lessons, the opportunity and that you pushed me out from my comfort zone so I could evolve.

I will also like to thank Prof. Pyeon and the staff at the Kyoto University Critical Assembly (KUCA), located at the Kyoto University Research Reactor Institute (KURRI) for the support and for having kindly provided the results of the kinetics experiment.

I could not forget my financial supporters during this thesis: KIT, the ÅForsk Foundation, and the Emma Berglunds Foundation. I am very grateful for your help, which made my life easier and my stay in Germany possible.

I also wish to extend my gratitude towards my colleagues at KIT for making my time in Germany more pleasant and letting me be a part of your group. I think I even will continue drinking espresso after this time! Finally, I must express my very profound gratitude to my parents, boyfriend and closest friends for providing me with unfailing support and continuous encouragement throughout my years of study and through the process of researching and writing this thesis. This accomplishment would not have been possible without them. Thank you all for helping me finally reach my goal I set up years ago.

List of Figures

1	Fission reaction where a neutron hit the target nucleus which split into two fission fragments and two to three neutrons. The process release about 200 MeV in every event.	1
2	Schematic of an ADS [8].	2
3	Radiotoxicity comparison between nuclear waste and transmuted fuel. The straight line at one represent neutrality, that there is no risk for harming the environment [8].	4
4	Computational scheme for transient calculation.	10
5	Schematic description of the structure of the method.	11
6	Layout of the KUCA for ADS experiments. The black line represent the indium wire used for measuring reaction rates. The grey square at I-15 represent the target of either D-T, W, W-Be or Pb-Bi.	12
7	Experimental configurations.	13
8	KUCA fuel assembly [17].	14
9	Unit cell fuel.	14
10	Direct flux for 172 and 40 energy groups.	15
11	System with the detector in the center (a) and with only polyethylene (b).	15
12	1D (R) model of the detector used for ECCO calculations.	16
13	Methodology for the generation of cross-sections of the KUCA control/safety rods.	17
14	Control rod C2 (also see Figure 6).	18
15	1D (R) model of control rod C2 used in ECCO.	18
16	System response to a external source can be divided into a prompt and delayed area.	21
17	Result case I3.	23
18	Result case I5.	23
19	Direct flux.	25
20	Adjoint flux.	26
21	Reaction rates for the three targets used during the experiment.	26
22	Normalized reaction rate for simulated deuterium-tritium source and one of the targets from the experiment.	26
23	Mean neutron generation time.	27
24	Comparison between simulations and measurements from detector 10U, in case I3.	28
25	Comparison between simulations and measurements from detector 15X, in case I3.	28
26	Comparison between simulations and measurements from the optical fiber detector, in case I3.	29
27	Comparison between simulations and measurements from detector 10U, in case I5.	30
28	Comparison between simulations and measurements from detector 15X, in case I5.	30
29	Comparison between simulations and measurements from the optical fiber detector, in case I5.	31

List of Tables

1	Number of inserted rods for case I3 and case I5.	12
2	Composition of fuel and polyethylene.	13
3	Correction of fluxes for 20 energy groups.	16
4	Layers in the 1D (R) ECCO model for the different control/safety rods.	18
5	Content of the control/safety rods [17].	19
6	Control rod worth calculated with VARIANT, and compared to the KUCA reference values and MCNP simulations. The k-effective with all the control/safety rods withdrawn, is used as reference of the reactivity, so it is not included. Completed inserted rod is described with 1, and withdrawn with 0.	19
7	ERANOS and PARTISN evaluation of the 3D (XYZ) geometry for the two core configurations, with k_{eff} reference from KUCA experiment.	20
8	Kinetic parameters and reference result for ERANOS/VARIANT and KIN3D/PARTISN for 40 energy groups.	20

Contents

1	Introduction	1
1.1	Fission as an energy source	1
1.2	The concept of ADS	2
1.3	Motivation for Accelerator Driven System (ADS)	3
1.4	Objective and structure of the thesis	4
2	Computational Methods for ADS	7
2.1	Direct and quasistatic methods for transient analysis of ADS	7
2.2	Description of codes employed	8
2.2.1	European Cell COde (ECCO)	8
2.2.2	European Reactor ANalysis Optimized System (ERANOS)	8
2.2.3	Variational Anisotropic Neutron Transport (VARIANT)	9
2.2.4	PARallel TIme-dependent SN code (PARTISN)	9
2.2.5	Computational scheme	9
3	The KUCA Reactor and its Modelling	11
3.1	The Kyoto University Critical Assembly (KUCA)	11
3.2	Neutron cross-section modelling	13
3.2.1	Fuel and reflector	13
3.2.2	Detectors	15
3.2.3	Control and safety rods	17
3.2.4	Static simulations	19
4	Area Method for Reactivity Estimation	21
4.1	Area method	21
4.2	Analysis of the PNS area method experimental results	22
5	Transient Analysis of Kinetics Experiments	25
6	Conclusion	33

1 Introduction

This chapter presents a general background of nuclear energy, the concept and motivation for accelerator driven system and last the structure of this thesis.

1.1 Fission as an energy source

Nuclear fission is a physical process such that a heavy nuclide is split into two lighter nuclides with release of energy. Fission reactions can either occur in a spontaneous way by radioactive decay, or be induced by bombarding a heavy atom with neutrons. The phenomenon was discovered by Otto Hahn and Fritz Strassmann in 1938, and theoretically explained by Lise Meitner and Otto Frisch in 1939 [1]. One very important element for fission is the fissile isotope ^{235}U . It is the second most common isotope of uranium in nature and has the ability to sustain a fission reaction. When a neutron impinges on a ^{235}U atom as in Figure 1, the absorption of the neutron leads to the splitting of the atom into two fission fragments and 2-3 neutrons. The total energy released in the reaction is about 200 MeV, and it comes from the kinetic energy of the fission fragments and emitted neutrons, and from gamma and beta radiation. Other isotopes that can be used for profitable energy production via nuclear fission, are ^{233}U , ^{239}Pu and ^{241}Pu [2]. The fact that new neutrons

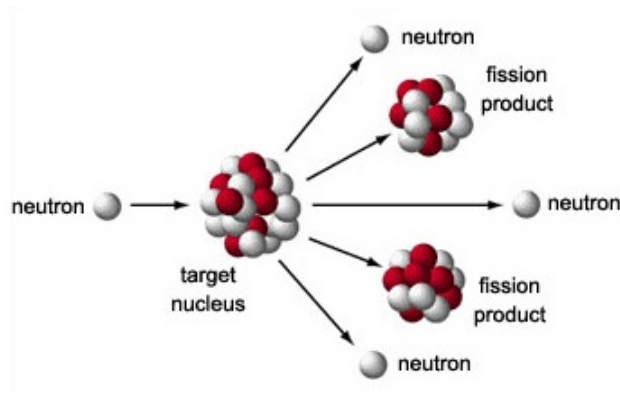


Figure 1: Fission reaction where a neutron hit the target nucleus which split into two fission fragments and two to three neutrons. The process release about 200 MeV in every event.

are emitted from each fission, allows a chain reaction to be maintained. This is one of the basic concept of a nuclear power reactor: given a proper amount of fissile material, a self-sustaining fission chain reaction can be established so that the neutrons lost are equal to the neutrons obtained from the fissions, and energy (that is eventually converted in electricity) can be generated at a stationary rate. Nowadays, the most common commercial nuclear facility is Light Water Reactors (LWRs) which can be either Pressurized Water Reactors (PWRs) or Boiling Water Reactors (BWRs). The nuclear fuel used in these reactors is manufactured using natural uranium. Natural uranium consists 0.7% ^{235}U (fissile) and 99.3% ^{238}U (non-fissile), which means that an enrichment of the fissile material is necessary (around 3%). Thermal reactors use a low-enriched fuel, which means that the neutrons have to be slowed down to thermal energies to maintain the fission. This is done by moderation, usually with water but also heavy water or graphite [2].

The first reactor was built in 1954 and in 2016 there were 450 LWRs in use and 60 more under construction. This corresponds to a power output of 392 GW and about 60 GW will come from the ones under construction [3]. The electricity demand world-wide is increasing, countries have a need for energy security and along with this an awareness of the climate threat is growing. Nuclear energy has minimal CO_2 emission and produced more than 11% of the worlds electricity in 2014 [4]. Yearly there is a production of approximately 20 ton nuclear waste per normal sized reactor, which sums up to 2000-2300 ton from the industry [5]. In nuclear waste only 3% of the mass is high level waste and thus contains 95% of the radioactivity [6].

The nuclear waste is separated into three categories, low-, intermediate- and high-level waste. The last mentioned, arises from the burning of the uranium in the reactor and in this process creating fission products, which some are long-lived. The half-life of the long-lived nuclides will determine how long the waste has to

be stored before it reaches a non-hazardous level. But, it is possible to reprocess the waste and separate the short- and long-lived fission products to reduce the waste volume, but not all countries do this. Not even all countries have a plan for the treatment of the high-level waste [7]. One solution to the constantly increasing waste volume would be to transmute the waste in Accelerator Driven Systems (ADSs). The waste can be reprocessed and used as fuel in ADS facilities, and with a high neutron yield transmutes the long-lived fission products into shorter lived ones. This is an option to close the fuel cycle and reuse the waste and at the same time gain more energy in the process.

1.2 The concept of ADS

The Accelerator Driven System (ADS) is a subcritical reactor coupled with a high-energy proton accelerator. An example of ADS is shown in Figure 2. That the system is subcritical essentially means that more neutrons are consumed than produced by fission, and the chain-reaction is maintained only with an external neutron source. Neutrons are provided to the system by spallation with the high-energy proton beam and a proper material placed in the center of the reactor. The nuclear material is placed all around the source since the neutrons spread isotropically. The system is then inherently safe because the chain reaction in the reactor dies out if the accelerator is turned off.

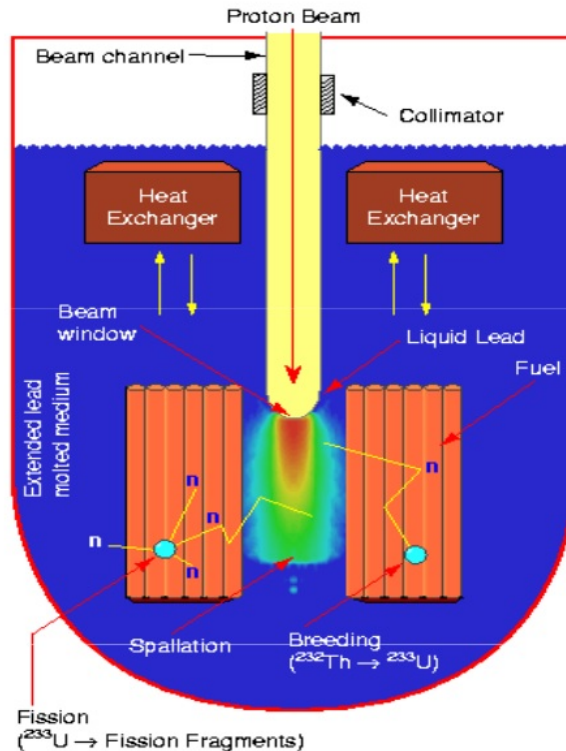


Figure 2: Schematic of an ADS [8].

The nuclear waste can be reprocessed and used as fuel in ADS. The system is designed to accommodate and burn large quantities of minor actinides and long lived fission products. A fuel with minor actinides only possesses a small fraction of delayed neutrons, thus possesses short half-life. The subcriticality is therefore a necessity to control the system with correct safety margins during operations. Since ADS have no critical condition to fulfill, almost any fuel composition can be used and more minor actinides can be burned, if the subcritical level is kept [8].

Appropriate cooling is needed in normal operations and in shutdown conditions (to cope with the removal

of decay heat). Different solutions have been investigated such as liquid metals as for example Pb, Pb–Bi or Na or gases like He or CO₂. These options are considered because of their thermal properties (improved heat transfer), which is required if electricity is to be produced efficiently. The gases have good chemical compatibility but their use requires high primary system pressure, 50-70 bars. This increases the possibility of structural failures with loss of coolant. Liquid metals, can operate close to atmospheric pressure but have strong chemical reactivity [8].

In order to use ADS for electricity production, the reactor needs to be connected to a system of turbines/electrical generator, similarly to the case of a LWR. Several technical issues must be investigated to make the ADS a viable option for the future. For example, should the proton beam be stable and without beam trips to have full control over the system, to avoid damage the reactor structure or the target which can lead to a change in plant parameters. This system also gives rise to new scenarios of nuclear accident which have to be considered since it is directly linked with the provision of neutrons. Another challenge is the fuel, as mentioned the goal is to burn a fuel with a high content of minor actinides, so further developments in the reprocessing of LWR spent fuel are needed for a better separation of the isotopes of interest.

1.3 Motivation for Accelerator Driven System (ADS)

When the nuclear fuel gets exhausted and is discharged from LWRs, it is highly radioactive because of the unstable fission products and because of the actinides produced by the neutron captures of ²³⁸U, like plutonium, neptunium and americium. Spent fuel from nuclear power plants is the main contributor to nuclear waste.

To deal with the spent fuel, two strategies can be followed. The first strategy is related to the so-called open fuel cycle, which refers to storing the nuclear waste in a safe repository and let it naturally decay. This option has two disadvantages, first the utilization of the nuclear fuel is not optimal, and secondly it can take a long time for the actinides to decrease their radio-toxicity to an acceptable level. The second strategy is based on a close fuel cycle, where spent fuel is reprocessed, and fissile and fertile materials can be recovered and re-used. One of the options under study for developing a close fuel cycle is to employ an Accelerator-Driven System (ADS) to transmute the actinides in less dangerous isotopes with shorter decay time.

If the fuel is to be recycled two main options is considered. One option is an integrated system for all NPPs (critical reactors as well as ADS) and to keep the Pu and minor actinides together and have homogeneous recycling in energy producing reactors. This means that minor actinides are distributed homogeneous in the fuel cycle. The fuel will after use be reprocessed and new fuel will be made of a mixture of U, Pu and minor actinides. The second choice is called "double strata" and here Pu would be separated from the minor actinides. Plutonium and uranium would be used in critical reactors while the minor actinides would be used in dedicated systems as ADS, and once again the waste would be reprocessed for fabrication of new fuel to close the cycle. In both cases, it should be known that minor actinides need special handling and precautions must be taken both during fabrication and reprocessing [8].

Both critical and subcritical reactors have been considered for the task of burning minor actinides but due to the characteristics of the fuel the safety barriers are too low for a critical system. The fact that the subcritical reactor uses a fast neutron spectrum is an advantage since the transuranic elements work as neutron sources, but would work as neutron poisons in a thermal reactor. In thermal reactors, the thermal neutrons enhance the content of high-mass isotopes instead of transmute them which is desired [8].

The subcritical system is as mentioned inherently safe which means that it cannot become supercritical, when the source is turned off so will the reactor. The fuel composition can be more flexible thanks to the subcriticality and almost any fuel can be loaded into the core. This opens other possibilities for the industry, for example the use of non-fissile material for fuel such as thorium. The other existing option today is to extract uranium and plutonium from the used fuel and reuse it in MOX fuel in LWRs. This is a difficult process with high expenses and the rest which cannot be reprocessed still goes to repositories for a long time since no minor actinides are destroyed in the process [9].

Depending on the total energy generated by the fuel i.e. the burnup, the composition in the waste will be different, but in general the storage time is about a million years. This is one reason to reprocess and transmute the waste, as in ADS. If the nuclear waste is transmuted the radiotoxicity will be lowered, see Figure 3, where level one in this figure represents a toxicity level which is not harmful to the environment [8].

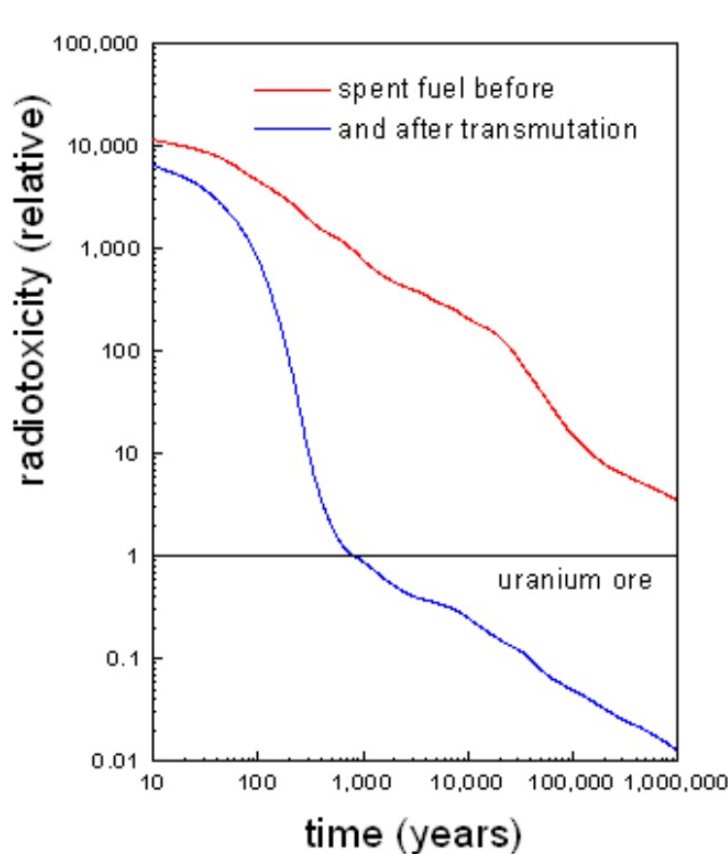


Figure 3: Radiotoxicity comparison between nuclear waste and transmuted fuel. The straight line at one represent neutrality, that there is no risk for harming the environment [8].

With recycling of the fuel less of earth resources will be spent and last longer. The risk to society will also be lowered since the fuel only need to be stored around five- to seven-hundred years. The associated risk at the disposal will be lowered because the waste has decreased its radiotoxic level after transmutation. The waste management within the nuclear community has still not been mastered and this is a way to close the fuel cycle and reuse the fuel. There are many large actors like the USA, Europe, Japan, South Korea, India, China and Russia and organization like IAEA are interested and support this idea [9].

1.4 Objective and structure of the thesis

Computer simulations are an important contribution to the design and safety analysis of nuclear reactors. The Accelerator Driven Systems (ADSs) are of interest to study since the external neutron source will introduce spatial effects on the neutron flux, which are very different from the fundamental mode in critical reactors. Validation and improvement of the kinetics models in the deterministic codes is done by benchmarking against kinetics experiments.

The aim of the thesis was to investigate and compare the performances of different transport codes by analyzing transient pulsed experiments in subcritical configurations. This has been done by investigating the Phase-I kinetics experiments performed at Kyoto University Critical Assembly (KUCA), located at the Kyoto University Research Reactor Institute (KURRI), for the two reactor configurations I3 and I5. The deterministic codes were used to predict both static and time-dependent cases from a detector-wise response from an external neutron pulse. The codes used in this work are PARTISN and ERANOS/VARIANT, both coupled to the KIN3D module for kinetic and perturbation calculations.

The thesis is structured as follows. In Chapter 2 an introduction to the deterministic codes and the methodology applied to the work is presented. Chapter 3 provide information about the analyzed reactor, KUCA, and how the cross-sections have been processed. Chapter 4 contains the explanation of the

area method and the results obtained from the application of the method. Chapter 5 discusses the time-dependent kinetic experiments performed at KUCA and comparison with the two simulation methods used, KIN3D/VARIANT and KIN3D/PARTISN. Last the conclusions are presented in Chapter 6.

2 Computational Methods for ADS

This chapter provide background information about calculation methods and codes used. Section 2.1 introduces the basics of direct and quasi-static methods for transient analysis of ADS. The following part, Section 2.2, the codes used are briefly discussed (ECCO, ERANOS, KIN3D/VARIANT and KIN3D/PARTISN) and how these are coupled.

2.1 Direct and quasistatic methods for transient analysis of ADS

The multigroup time-dependent transport equation [10] with the assumption that the scattering term and the external neutron source are isotropic, can be written as

$$\begin{aligned} \frac{1}{v_g(\mathbf{r},t)} \frac{\partial}{\partial t} \psi_g(\mathbf{r},\mathbf{\Omega},t) + \mathbf{\Omega} \nabla \psi_g(\mathbf{r},\mathbf{\Omega},t) = \frac{1}{4\pi} \sum_{g'} \Sigma_{s,g' \rightarrow g}(\mathbf{r},t) \phi'(\mathbf{r},t) \\ + \frac{1}{4\pi} \left[\chi_g(\mathbf{r},t) - \sum_i \chi_{i,g} \beta_i(\mathbf{r},t) \right] F(\mathbf{r},t) + \frac{1}{4\pi} \sum_i \lambda_i \chi_{i,g} C_i(\mathbf{r},t) + \frac{1}{4\pi} S(\mathbf{r},t) \end{aligned} \quad (1)$$

where F is the fission source term which can be written as

$$F(\mathbf{r},t) = \frac{1}{\gamma} \sum_{g'} \nu \Sigma_{f,g'}(\mathbf{r},t) \phi_{g'}(\mathbf{r},t) \quad (2)$$

where γ represent k-effective for a homogeneous problem or for an external source problem. The delayed neutron fraction, β_i , for family i and group g can be written as

$$\beta_i(\mathbf{r},t) = \frac{\sum_{g'} \beta_{i,g'}(\mathbf{r},t) \nu \Sigma_{f,g'}(\mathbf{r},t) \phi_{g'}(\mathbf{r},t)}{\sum_{g'} \nu \Sigma_{f,g'}(\mathbf{r},t) \phi_{g'}(\mathbf{r},t)}. \quad (3)$$

The other terms in Equation 1 are as follows, ψ_g represent the angular neutron flux for energy group g for $g = 1,2,\dots,G$, ϕ is the scalar neutron flux, Σ is the macroscopic cross-section, λ_i is the decay constant for family i , χ is the fission spectrum including both prompt and delayed neutrons, S represent the external source and C_i is the concentration of delayed neutron precursors for family i as

$$\frac{\partial}{\partial t} C_i(\mathbf{r},t) = \beta_i(\mathbf{r},t) F(\mathbf{r},t) - \lambda_i C_i(\mathbf{r},t). \quad (4)$$

For each time step in Equation 1, are the neutron cross-sections, external prompt and delayed source data provided with KIN3D to the transport solver, VARIANT or PARTISN.

In order to perform transient simulations within a reasonable computational time Equation 1 with related equations can be solved by applying, for instance, direct and quasistatic methods. To start the transient calculations the initial assumption is that the reactor is in steady state. According to [11], if it is assumed that the flux distribution and the concentrations of precursors are known at time t_0 , the flux distribution at time t_1 can be approximated as

$$\psi_g(\mathbf{r},\mathbf{\Omega},t_1) \approx P(\mathbf{r},t) [\psi_g(\mathbf{r},\mathbf{\Omega},t_0) + \alpha_g(\mathbf{r},\mathbf{\Omega})(t - t_0)] \quad (5)$$

where $P(r,t)$ is an amplitude function of the neutron flux which at time t_0 is equal to unity, ψ is the flux shape and α_g is an unknown variable. KIN3D coupled with one of the transport solver VARIANT or PARTISN have four kinetic options which can be employed, direct, improved quasistaic, adiabatic and point kinetic. For the **point kinetic option** the flux shape is constant, since the solution is the same in the whole reactor. The **direct option** assumes that in each time step the flux changes linearly, and gives the flux as a product of an exponential function and a linear flux shape. The exponential function is evaluated by KIN3D from flux variation computed in the past. For the **improved quasistatic** method the flux shape has to be updated during the transient calculation.

If the time interval is chosen to be small enough the amplitude function, $P(r,t)$, can be taken as any smooth function without interfering on the accuracy, and the Equation 5 can be written

$$\alpha_g(\mathbf{r},\mathbf{\Omega}) = \frac{1}{\Delta t} \left[\frac{1}{P(\mathbf{r},t_1)} \psi_g(\mathbf{r},\mathbf{\Omega},t_1) - \psi_g(\mathbf{r},\mathbf{\Omega},t_0) \right] \quad (6)$$

where $\Delta t = t_1 - t_0$. By employing this in Equation 5 for $t = t_1$

$$\frac{\partial}{\partial t} \psi_g(\mathbf{r},\mathbf{\Omega},t_1) = \left[\frac{\frac{\partial}{\partial t} P(\mathbf{r},t_1)}{P(\mathbf{r},t_1)} + \frac{1}{\Delta t} \right] \psi_g(\mathbf{r},\mathbf{\Omega},t_1) - \frac{1}{\Delta t} P(\mathbf{r},t_1) \psi_g(\mathbf{r},\mathbf{\Omega},t_0) \quad (7)$$

and the delayed neutron fraction can also be assumed to linearly depend on time which gives

$$\beta_i(\mathbf{r},t)F(\mathbf{r},t) \approx P(\mathbf{r},t) [\beta_i(\mathbf{r},t_0)F(\mathbf{r},t_0) + a_i(\mathbf{r})(t - t_0)] \quad (8)$$

where

$$a_i(\mathbf{r}) = \frac{1}{\Delta t} \left[\frac{1}{P(\mathbf{r},t_1)} \beta_i(\mathbf{r},t_1)F(\mathbf{r},t_1) - \beta_i(\mathbf{r},t_0)F(\mathbf{r},t_0) \right] \quad (9)$$

and then the precursor can be obtained by integrating

$$\frac{\partial}{\partial t} C_i(\mathbf{r},t) = P(\mathbf{r},t) [\beta_i(\mathbf{r},t_0)F(\mathbf{r},t_0) + a_i(\mathbf{r})(t - t_0)] - \lambda_i C_i(\mathbf{r},t). \quad (10)$$

2.2 Description of codes employed

Multigroup deterministic codes have been used for analyzing the KUCA subcritical reactor. This section will first provide a separate description of the different codes, followed by a description of the coupling procedure of the codes employed.

2.2.1 European Cell COde (ECCO)

The European Cell COde (ECCO) solves [12] the integral transport equation in an infinite lattice using multigroup cross sections with fine energy structure and accurate geometry representation. ECCO also considers inelastic, elastic and (n, xn) group-to-group transfer cross sections. For the most important nuclides the energy structure consists of 1968 groups, this fine energy spectrum goes up to 20MeV, but can be collapse into coarser energy groups (33 or 172) to save computational time. These multigroup self-shielded neutron cross-sections are then used in the core geometry defined by ERANOS (Section 2.2.2). Several cross-sections libraries are available i.e. JEFF, JENDL, ENDF.

2.2.2 European Reactor ANalysis Optimized System (ERANOS)

The European Reactor ANalysis Optimized calculation System (ERANOS) [13] is a deterministic computational platform which includes different types of solvers and methods to simulate reactor cores in 3D (XYZ, HEX-Z), 2D (RZ, XY) or 1D geometries. ERANOS offers different methods, namely direct, improved quasi-static, adiabatic and point kinetic option. The point kinetic option is used for computing the time-dependent flux. The space-time dependent flux can be estimated by applying the direct and quasi-static option. The quasi-static approach can also be used to calculate the variation of reactivity and mean neutron generation time in transient conditions.

2.2.3 Variational Anisotropic Neutron Transport (VARIANT)

Variational Anisotropic Neutron Transport (VARIANT) [14] [15] is an extension of the ERANOS code which is used as solver for the time-dependent transport equation for the same geometries used in ERANOS. VARIANT solves the transport equation by a variational nodal method and spherical harmonics (P_N method) are used to treat the angular variables. A given function which is continuous in space can be extended by spherical harmonics, namely Legendre polynomials.

2.2.4 PARallel TIme-dependent SN code (PARTISN)

The PARallel TIme-dependent SN code (PARTISN) [11] [16] is a deterministic code that solves the static and time-dependent Boltzmann transport equation according to a multigroup discrete ordinates approach. In this code, no model for delayed neutrons is included, and therefore an extension was made at KIT/IKET to couple the code with KIN3D. KIN3D is a kinetics and perturbation extension of the VARIANT/TGV nodal transport code available in ERANOS. This means, that the PARTISN code can perform both static and time-dependent calculations, the last mentioned by employing the direct scheme. KIN3D/PARTISN can be used as a transport solver instead of KIN3D/VARIANT. But, PARTISN uses a discrete ordinates method (S_N) to treat the angular variables.

2.2.5 Computational scheme

The computational scheme relies on the coupling of the codes introduced above, and it is illustrated in Figure 4. As a first step, multigroup self-shielded micro- and macroscopic cross-sections are processed by ECCO and provided to ERANOS to be used in the core geometry. The cross-sections are collapsed from a fine energy spectrum down to a coarser scheme with fewer groups and homogenized, so that they can be used for 3D (XYZ) full core calculations.

Cross-sections, external neutron source and geometry are processed in ERANOS, which can be coupled with either the PARTISN or VARIANT code which solves the transport equation for the chosen geometry. These codes are also coupled with KIN3D [10] which is a kinetic and perturbation extension of the VARIANT code. So, KIN3D coupled with VARIANT or PARTISN solves the time-dependent transport equation and performs perturbation calculations in geometries XY, XYZ and HEX-Z. The deterministic codes [10] use outer iteration technique for solving the steady-state Boltzmann equation to be able to transform the initial multigroup problem into a sequence of one group problems with an external source.

As described in Figure 4, to simulate the transient the transport solver (PARTISN or VARIANT) must first be used to calculate the initial flux, ψ_g , and the adjoint flux, ψ_g^* . These fluxes are then provided to KIN3D as input to start the transient. ψ_g is in KIN3D used to compute precursor concentration, the external delayed source and fission spectrum. The adjoint is used as a weighting function for the system to evaluate the importance of the flux.

At each time step the fission spectrum and the delayed neutron source are recalculated and external files are generated by KIN3D and supplied to the transport solver for a new calculation. In this way the prompt fission spectrum is updated and provided to the transport solver again, which then updates the ψ_g . The procedure is repeated until the end of the transient. The parameter of interest such as reactivity or power distribution are then provided to the output file.

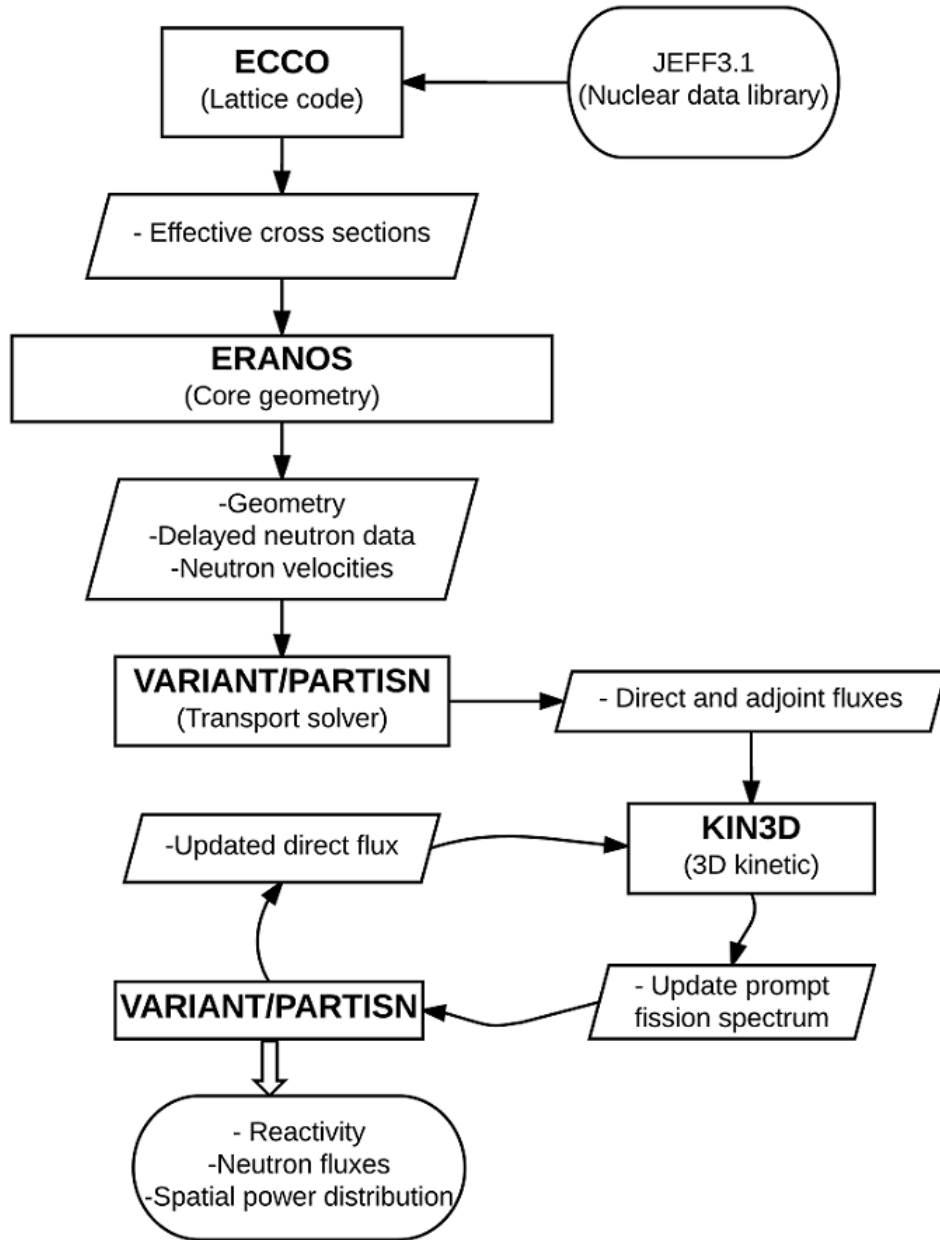


Figure 4: Computational scheme for transient calculation.

3 The KUCA Reactor and its Modelling

These sections follow the methodology in Figure 5. So, first are all cross-section processed in a 2D model with ECCO, which are then used in a 3D (XYZ) assessment of the KUCA reactor with ERANOS. This model is first analyzed for the steady state case with VARIANT and PARTISN, and compared with the KUCA references. When reasonable agreement with references are found, the same model is used for analysing the transient case with KIN3D/VARIANT and KIN3D/PARTISN. Section 3.1 describes the Kyoto University Critical Assembly (KUCA). This is presented first to give an understanding for the following Section 3.2, which contains the description of the cross sections processing for the model. The processing of the cross-sections are divided into different parts; Section 3.2.1 for fuel and reflector, Section 3.2.2 for the detectors, Section 3.2.3 for the control and safety rods. Last is Section 3.2.4 which presents the static result for the 3D (XYZ) model for case I3 and case I5. The transient analysis is presented in Section 5.

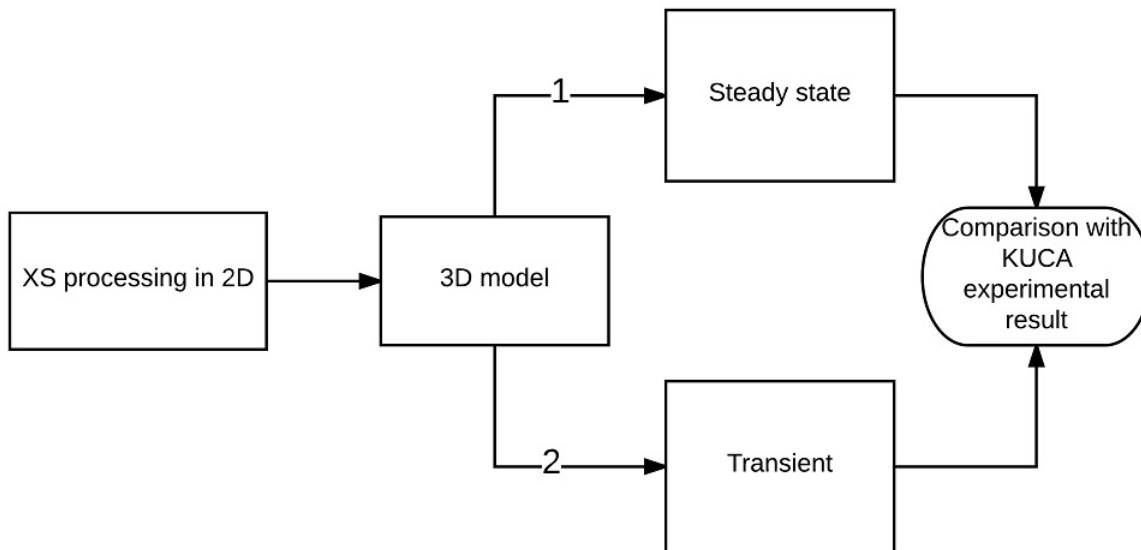


Figure 5: Schematic description of the structure of the method.

3.1 The Kyoto University Critical Assembly (KUCA)

KUCA [17] is a multi-core type critical assembly located at the Kyoto University Research Reactor Institute (KURRI) in Japan. This facility has been used for basic research on reactor physics, such as critical experiments on highly-enriched uranium cores, nuclear characteristics of thorium fueled reactor, and more. Furthermore, experiments related to ADS were also carried out in KUCA. A schematic figure of the core is found in Figure 6. It is a zero-power reactor with a subcritical core configurations coupled with a Fixed-Field Alternating Gradient Accelerator (FFAG) with Cockcroft-Walton pulsed neutron generator. With a FFAG accelerator 100 MeV protons were injected with 1 nA intensity with a pulsed frequencies of 20 Hz. The accelerated protons hit a target of W, W-Be or Pb-Bi (44.5% Pb and 55.5 Bi%) to generate high-energy neutrons through spallation. The targets were placed in *H15* (the gray square) in Figure 6. The size of target was decided from previous analyses and the resultant neutron yield created was about $1.0 \cdot 10^8$ 1/s.

The nuclear core consisted of 21 to 25 fuel assemblies. Details of the fuel assembly are shown in Figure 7a and 7b. KUCA used highly-enriched uranium-aluminum (U-Al) alloy core surrounded by polyethylene. The lower and upper parts of the fuel element were polyethylene reflector regions. The core was surrounded by 60 cells of 3.1 mm thick polyethylene plates, which served as both reflector and moderator. Three control rods and three safety rods can be used to adjust the reactivity level and to shut the reactor down. Three detectors were used, two of them were BF_3 detectors and one an optical fiber detector (LiF+ZnS) to monitor prompt and delayed neutrons. The black wire in Figure 6 is an indium wire for measuring the reaction rates. The core itself had a active height of 400 mm.

KUCA experimental data as well as the specifications of the core have been used as references for the construction of the model. To simulate the system ECCO was used with JEFF3.1 nuclear library for neutron cross-section processing. In ERANOS a 3D (XYZ) geometry was employed with a mesh size of 5 cm, which is the same length order as the neutron mean free path. Two different control rod configurations with the aim of investigating the reactivity feedback are seen in Figure 7a (case I3) and 7b (case I5). In Table 1, the number of inserted rods for the two configurations are described. The source in the calculations is described by a deuterium-tritium source of 14 MeV and placed at target position (grey box in Figure 6). In the static analyses, VARIANT and PARTISN were used for solving nodal multigroup transport equations applied to the system. KIN3D/VARIANT and KIN3D/PARTISN were used to model the transient behavior of the core and the delayed neutron behavior. The system was divided into sub-regions taking into account the geometrical heterogeneities. The continuous energy spectrum was divided into 40 energy groups for both VARIANT and PARTISN.

Table 1: Number of inserted rods for case I3 and case I5.

Case	Rod insertion
I3	C1, C2, C3, S4, S5, S6
I5	C1, C2, S4, S6

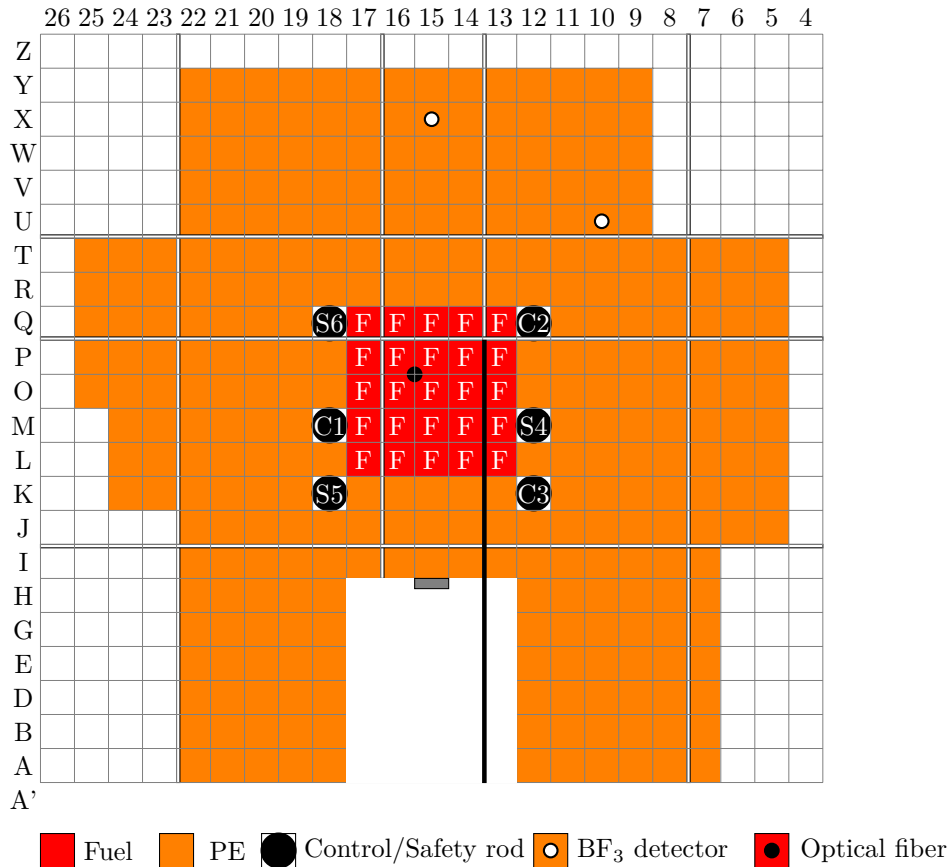


Figure 6: Layout of the KUCA for ADS experiments. The black line represent the indium wire used for measuring reaction rates. The grey square at I-15 represent the target of either D-T, W, W-Be or Pb-Bi.

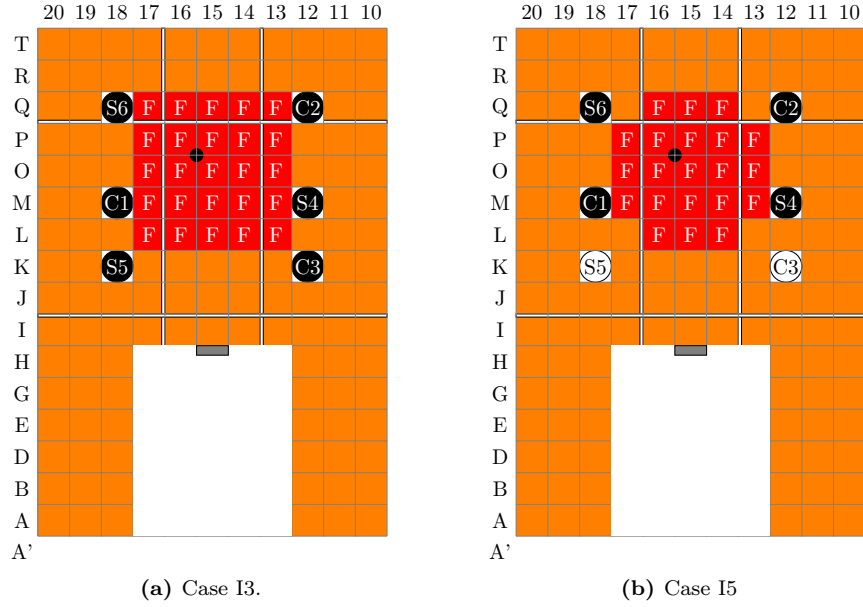


Figure 7: Experimental configurations.

3.2 Neutron cross-section modelling

In the following sections the treatment of the cross sections for the model will be explained. The Section 3.2.1 is dedicated to the processing of the fuel and the reflector, Section 3.2.2 to the detectors and Section 3.2.3 to the control/safety rods.

3.2.1 Fuel and reflector

To create multigroup self-shielded macroscopic cross sections for the KUCA fuel assemblies, an ECCO lattice transport calculation is carried out over a 2D unit cell. These cross sections are provided to ERANOS where the core geometry is described. For each material region in the core the composition needs to be specified with the cross sections.

To process the cross sections with ECCO compositions of the materials are first specified. These are then used for describing environments which thereafter are used in unit cells to process cross sections. For the fuel assemblies the composition of the fuel and polyethylene are specified from KUCA [17] and given in Table 2.

Table 2: Composition of fuel and polyethylene.

Fuel		Polyethylene	
	Atomic density [$10^{24}/\text{cm}^3$]		Atomic density [$10^{24}/\text{cm}^3$]
^{234}U	1.3659E-5	CO	4.00042E-2
^{235}U	1.50682E-3	HC	8.00083E-2
^{236}U	4.82971E-6		
^{238}U	9.25879E-5		
^{27}Al	5.56436E-2		

These compositions are used to create environments. For example, a fuel environment is composed of 100% fuel material (composition from Table 2) and PE is composed of 100% polyethylene. To create the cladding which surrounds the fuel assemblies, the environment is composed of 34% air material and 66% ^{27}Al material. These environments are then used to describe cells. For example, the fuel assembly in KUCA

(Figure 8) is described by cells. One unit cell is composed of one plate of polyethylene and one plate of fuel. To recreate this with reflective boundary condition in ECCO the polyethylene plate is split into half and placed as in Figure 9. This should also be surrounded with cladding, and to get the proper cross section from this cell the cladding is placed on the top and bottom with the same area as the left figure in Figure 8.

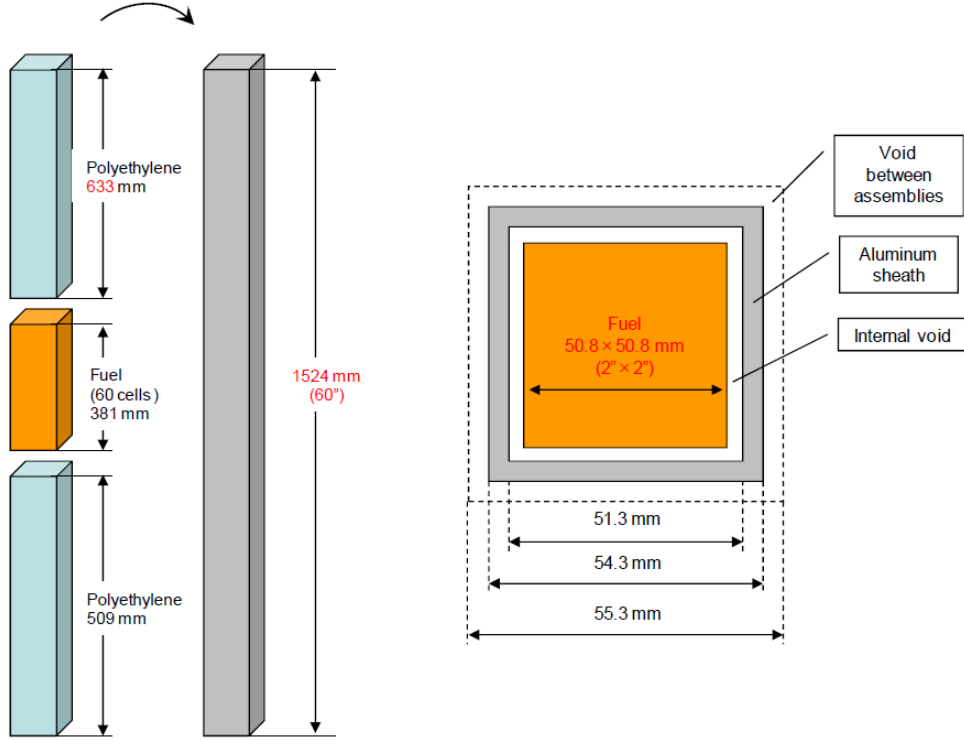


Figure 8: KUCA fuel assembly [17].

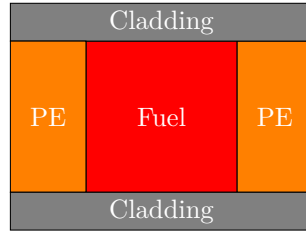


Figure 9: Unit cell fuel.

To obtain the cross section the transport equation is solved for these cells in the 2D geometry with reflected boundary conditions for 40 energy groups. The flux for one unit cell for 40 energy groups does not deviate considerably from the original 172 groups, see Figure 10. Full core calculations require few energy groups and coarser spatial meshes to have a practical computational time. Therefore, the macroscopic cross-sections generated with ECCO are condensed in energy and homogenized over the cell.

The cross sections are homogenized and condensed as a function of energy to preserve the reaction rates

$$\sigma_{x,i}^g = \frac{\int_g \sigma_{x,i}(E)\phi(E)dE}{\int_g \phi(E)dE}, \quad (11)$$

and this multigroup self-shielded cross sections can then be used in the 3D (XYZ) geometry in ERANOS.

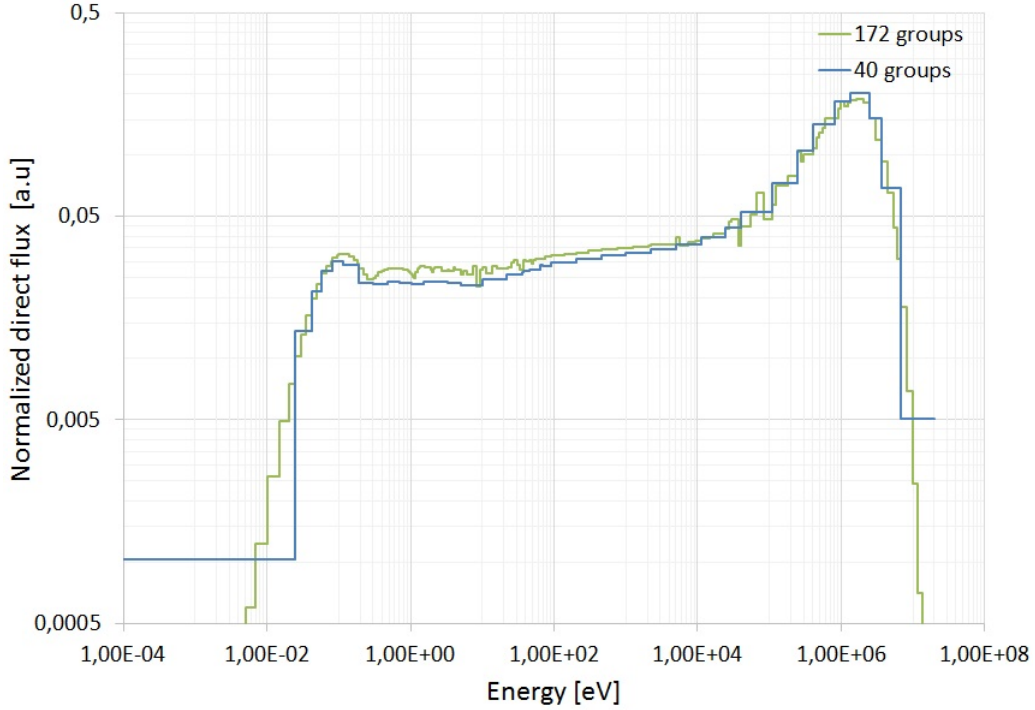


Figure 10: Direct flux for 172 and 40 energy groups.

3.2.2 Detectors

Two types of detectors were used in the reactor, one fiber detector in the fuel region and two BF_3 detectors in the reflector region. The fiber detector was neglected because of its small volume. The two detectors in the reflector region were of considerably larger volume and needed to be properly modelled, otherwise the discrepancies between simulated and real neutron flux may become severe. To investigate the impact on the neutron flux from the BF_3 detector two VARIANT simulations were run, one with the detector and one without. The detectors consisted mostly of air and only a very small volume of BF_3 , so this volume were documented as plain air. Figure 11 describes the two systems used for the simulations, the left figure describes the system with detector where the detector volume is given as plain air, in the right figure the detector is substituted with polyethylene.

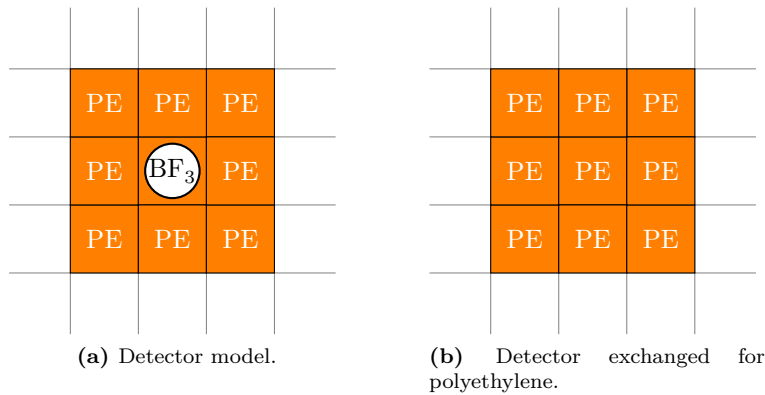


Figure 11: System with the detector in the center (a) and with only polyethylene (b).

First the cross-sections are generated with ECCO, in a 1D (R) model. The center of the fuel region in

the 3D (XYZ) KUCA model has been assumed the center of the 1D (R) ECCO model. The model used is given in Figure 12 where the area of each region is the same as the area of the surrounding fuel assemblies. A homogenized mixture of materials is employed. For ECCO calculation, the void and reflective boundary conditions have been imposed on R and Z, respectively. The region-wise self-shielded neutron cross-sections for 20 energy groups have been computed and employed in the equivalent 2D (XY) VARIANT model. The results of the two simulations are reported in Table 3. An energy-wise correction factor was then estimated by taking the ratio between the two neutron fluxes. These correction factors can be applied to the transient calculations in such a way that the presence of the detectors can be taken in account.

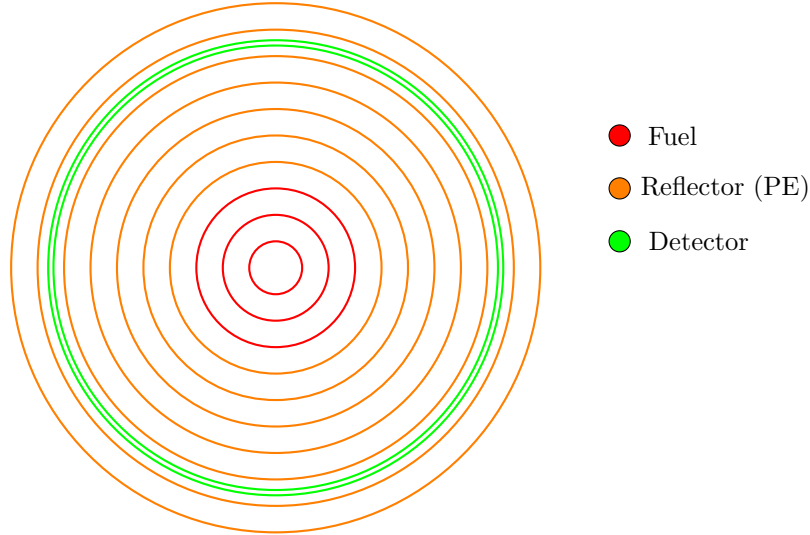


Figure 12: 1D (R) model of the detector used for ECCO calculations.

Table 3: Correction of fluxes for 20 energy groups.

Energy [eV]	Neutron flux [n/cm ² s], with detector (air)	Neutron flux [n/cm ² s], no detector (PE)	Energy-wise correction factor
19.30	17209	16114	1.06795
6.700	63439	43047	1.47371
2.470	51196	27769	1.84364
1.350	33374	15874	2.10243
0.821	33723	15585	2.16381
0.408	16859	8161	2.06577
0.247	18510	9644	1.91939
0.111	21981	12458	1.76441
2.48E-2	9086	5492	1.65450
1.11E-2	15999	10184	1.57099
2.25E-3	14698	9892	1.48577
4.54E-4	13860	9823	1.41100
9.17E-5	12654	9499	1.33201
1.95E-5	19904	15767	1.26238
1.50E-6	13945	11744	1.18741
3.00E-7	22604	34952	0.64672
1.15E-7	46021	116500	0.39503
5.80E-8	21822	69605	0.31351
4.20E-8	25134	91454	0.27483
2.50E-8	21296	97687	0.21800

3.2.3 Control and safety rods

The control rods are usually placed in a symmetrical way in a reactor, which is not the case for the two core configurations of KUCA. This means that each control/safety rod must be separately treated to get the correct reactivity feedback. As seen in Figure 7a and 7b, either the control rods (labelled as 'C') or the safety rods (labelled as 'S') are not positioned symmetrically and they are surrounded by fuel and reflector material in different manners. Nevertheless, there are some equivalences between control and safety rods, such as: S5 and C3; S4 and C1; and S6 and C2. The similar rods are surrounded by the same amount of fuel and reflector material. It is very important to simulate this feedback in a good manner since ADS are characterized by strong neutron flux gradients, and so by strong spatial effects. One method [18] that can be used to evaluate the correct feedback from the control rods, is to adjust the ^{10}B content. Such a procedure is described in Figure 13.

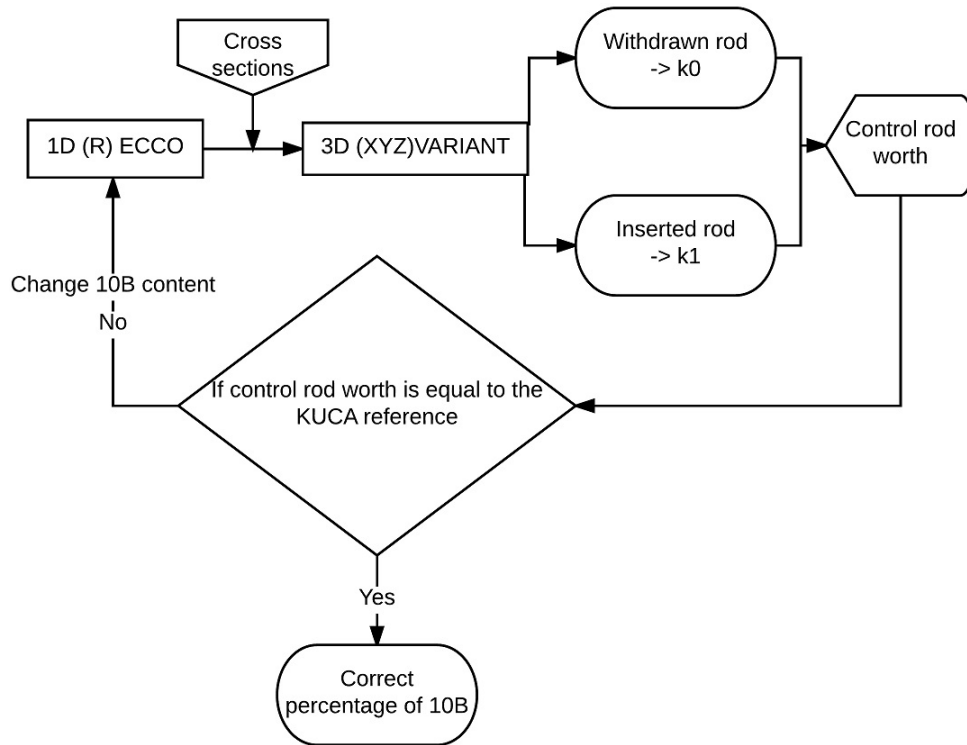


Figure 13: Methodology for the generation of cross-sections of the KUCA control/safety rods.

First each control rod was described in a 1D (R) model in ECCO to get the cross sections needed in VARIANT. The control/safety rods were separated into the three cases (S5 and C3; S4 and C1; and S6 and C2). For example is the upper control/safety rods (S6 and C2) is given in Figure 14 surrounded by two fuel assemblies and six polyethylene (reflector) assemblies. In ECCO this can be described as in Figure 15 with the corresponding areas.

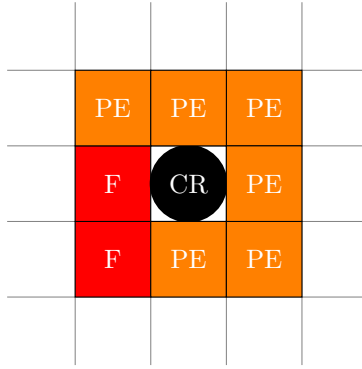


Figure 14: Control rod C2 (also see Figure 6).

In Table 4 each layer starting from the center of the control rod are described for the three cases of control/safety rods. The colors for the upper control rod correspond to the colors of the ring in Figure 15, starting from the center of the control rod. To get a correct reactivity feedback from the lower control/safety rod (S5 and C3), two fuel assemblies (instead of only one) were used, but placed further away from the rod. In all models the *fuel* in Table 4 is a mixture of 42.19% fuel, 42.2% polyethylene, 10.3% aluminum and 5.31% air. The layer called *PE* is polyethylene and *CR* refer to the control rod consist of 29.36% of the original control rod content, 23.97% aluminum and 46.68% air. The original content for the control rod is found in Table 5.

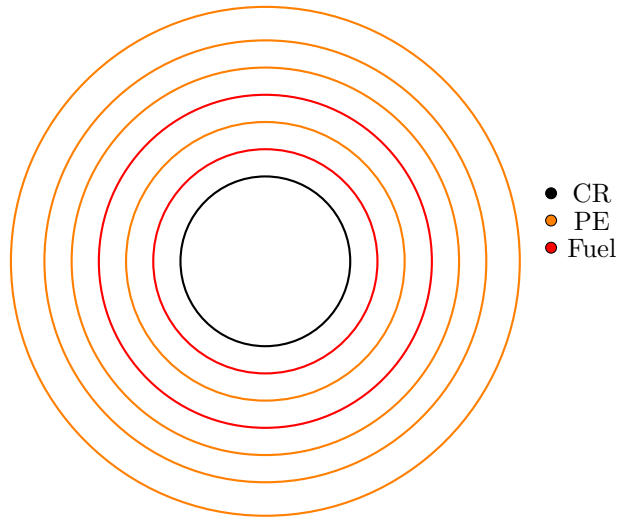


Figure 15: 1D (R) model of control rod C2 used in ECCO.

Table 4: Layers in the 1D (R) ECCO model for the different control/safety rods.

Radius [cm]	S5 & C3	S4 & C1	S6 & C2
3.119	CR	CR	CR
4.119	PE	Fuel	Fuel
5.119	PE	PE	PE
6.119	Fuel	Fuel	Fuel
7.119	PE	PE	PE
8.119	Fuel	Fuel	PE
9.35	PE	PE	PE

Table 5: Content of the control/safety rods [17].

Isotope	$[\times 10^{24}/\text{cm}^3]$
^{10}B	$3.87448 \cdot 10^{-3}$
^{11}B	$1.68447 \cdot 10^{-2}$
^{16}O	$3.10787 \cdot 10^{-2}$

The self-shielded neutron cross sections from ECCO were then used in a 3D (XYZ) model in VARIANT for core configuration I3 (Figure 7a). Two simulations were performed as described in Figure 13, one with the control rod and one without to obtain two k-effective values. With these k-effective values the reactivity control rod worth was calculated as

$$\Delta\rho = \frac{k_1 - k_0}{k_1 \cdot k_0} \quad (12)$$

where k_1 and k_0 represent the k-effective for inserted and withdrawn rod. The reactivity was then for the three control rod cases compared with the KUCA reference [17]. If the reactivity was not within $\pm 10\%$ of the KUCA reference, the ^{10}B content was then altered in the homogenized model, and the procedure repeated as described in Figure 13. The result can be found in Table 6.

KUCA only had references for one control/safety rod inserted at a time. To further investigate the reactivity feedback with the new cross sections for the control rods, a MCNP model for the reactor was created as reference. The reactivity was calculated with MCNP and VARIANT for the fuel arrangement in case I3 for the matrix of inserted/withdrawn rods described in Table 6. In this table, also the KUCA reference [17] values are stated. The control rod worth computed by VARIANT with different control rod arrangements show an acceptable agreement with the reference MCNP results. This validate that the cross sections with the given percentage of ^{10}B are processed in a good way, given that there is not references from KUCA for all of the matrix but it is still on good agreement with MCNP.

Table 6: Control rod worth calculated with VARIANT, and compared to the KUCA reference values and MCNP simulations. The k-effective with all the control/safety rods withdrawn, is used as reference of the reactivity, so it is not included. Completed inserted rod is described with 1, and withdrawn with 0.

^{10}B content	14% S5 & C3	10% S4 & C1	4% S6 & C2	VARIANT $\Delta\rho$ [pcm]	KUCA rod worth [pcm]	Difference from KUCA [pcm]	MCNPX $\Delta\rho$ [pcm]	Difference from MCNPX [pcm]
1	1	1	1	-2990			-3260	270
0	1	1	1	-2803			-3035	232
1	0	1	1	-1166			-1089	-77
1	1	0	0	-2003			-2036	33
1	0	0	0	-230	-278	-48	-250	20
0	1	0	0	-1826	-1610	216	-1786	-41
0	0	1	1	-1250	-1192	58	-1089	-162

3.2.4 Static simulations

When all necessary cross-sections were processed, they were used in the 3D (XYZ) model of the system to investigate if the assessment agreed with the KUCA reference. The two core configurations were evaluated for 40 energy groups with both VARIANT and PARTISN and the result are reported in Table 7. The k_{eff} reference comes from the KUCA experiment and agrees with the simulated results for both Case I3 and Case I5. The kinetic parameters calculated with means of ERANOS/VARIANT and KIN3D/PARTISN are shown in Table 8. Result for β_{eff} show reasonable agreement for both simulation methods to the KUCA reference. There is a deviation from the KUCA result with approximately 20 pcm, but this is small. Furthermore, the mean neutron generation time was calculated for ERANOS/VARIANT and KIN3D/PARTISN which is in agreement with the KUCA reference.

Table 7: ERANOS and PARTISN evaluation of the 3D (XYZ) geometry for the two core configurations, with k_{eff} reference from KUCA experiment.

k_{eff} from	Case I3	Case I5
VARIANT	0.97013	0.95401
PARTISN	0.97116	0.95294
KUCA reference	0.97182	0.95327

Table 8: Kinetic parameters and reference result for ERANOS/VARIANT and KIN3D/PARTISN for 40 energy groups.

Parameter	ERANOS/VARIANT	KIN3D/PARTISN	KUCA Reference
β_{eff} [pcm]	829.2	827.1	807
Λ [s]	3.027E-5	3.032E-5	3.050E-5

4 Area Method for Reactivity Estimation

Section 4.1 gives the basics of the area method used for calculating the reactivity. Section 4.2, presents the results for the method applied to both experiments and simulations for the cases I3 and I5.

4.1 Area method

A method used to calculate the reactivity in a subcritical system is the area method, also referred to as "the Sjöstrand method" [19]. The response of a subcritical system to an external neutron pulse can be divided into a prompt and delayed contribution as illustrated in Figure 16. The prompt neutrons will follow the shape of the source pulse (the red area) and the delayed neutrons (which do not follow the variations of the source) will form a constant density assuming that an equilibrium of the precursors are reached (blue area). The ratio of the two areas is related to the system reactivity.

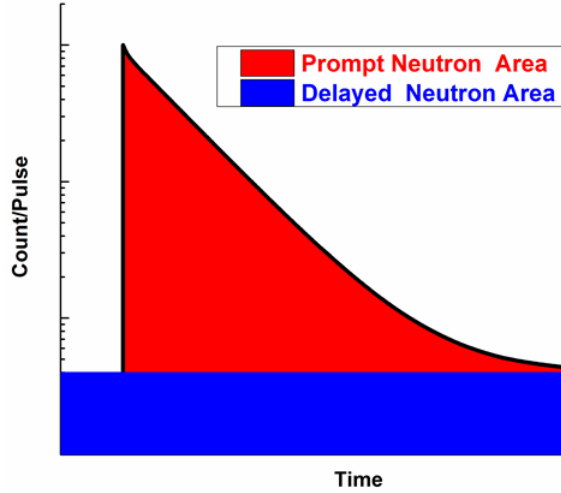


Figure 16: System response to a external source can be divided into a prompt and delayed area.

According to [20], the two areas of interest can be identified by making use of the inhomogeneous time-independent transport equation which can be re-written to the point kinetics with an external neutron source

$$\frac{d\phi}{dt} = \frac{\rho - \beta_{eff}}{\Lambda} \phi + \lambda C + S(t) \quad (13)$$

$$\frac{dC}{dt} = \frac{\beta_{eff}}{\Lambda} \phi - \lambda C \quad (14)$$

where ϕ is the total neutron flux, C is the delayed precursors, Λ is the neutron generation time, $S(t) = S_0 \delta_+(t)$ and represents a pulsed neutron source, and λ is the decay constant of the delayed neutron precursors.

This can be separated into prompt and delayed part (with the source belonging to the prompt) and integrated over time period T . The two areas are then equal to

$$A_p = \frac{S_0 \Lambda}{\beta_{eff} - \rho} \quad (15)$$

and

$$A_d = -\frac{S_0 \Lambda \beta_{eff}}{\rho(\beta_{eff} - \rho)}. \quad (16)$$

The ratio between equation 15 and 16, gives the absolute reactivity in dollars as

$$\frac{A_p}{A_d} = -\frac{\rho}{\beta_{eff}} = -\rho(\$), \quad (17)$$

where A_p represents the prompt area and A_d the delayed area in Figure 16.

It is not always possible to describe the system with the point kinetic approximation, but according to [21] a detector-wise reactivity may be evaluated which takes into account the spatial effects. The detector-wise reactivity is evaluated by performing two inhomogeneous time-independent (with external source) calculations. One for the prompt neutron area, A_p , by computing the time-integrated prompt neutron flux ϕ_p , and a second calculation to compute the delayed area, A_d , by computing the time-integrated total neutron flux, ϕ_t , and subtracting the prompt neutron flux. This gives

$$-\rho = \frac{A_p}{A_d} = \frac{\iiint \sigma_{detector} \tilde{\phi}_p dV dE d\Omega}{\iiint \sigma_{detector} (\tilde{\phi}_t - \tilde{\phi}_p) dV dE d\Omega} \quad (18)$$

where $\sigma_{detector}$ is the microscopic cross section of the detector.

4.2 Analysis of the PNS area method experimental results

As mentioned in Section 3.1, two core configurations were investigated, namely case I3 (Figure 7a) and case I5 (Figure 7b). A deuterium-tritium source of 14 MeV was added to the geometry at the target position, and the system response was analyzed by a detector dependent response. The detectors were positioned as in the KUCA experiment at 15X, 10U and optical fiber in the fuel region. The cross sections found for the BF_3 detectors and control/safety rods were used in the model. The experimental results have been analyzed with the method described in Section 4. The reactivity could be calculated with the "area method" as

$$\rho = -\frac{A_p}{A_d} \beta_{eff} \quad [pcm] \quad (19)$$

where A_p is the prompt area, A_d is the delayed area and β_{eff} is the effective neutron fraction. In Figure 17 and 18 the result from the experiments is presented for the three different targets with W , $W\text{-Be}$ and $Pb\text{-Bi}$. These experimental results are compared with the static calculations performed with ERANOS and PARTISN for 40 energy groups. The simulation results are also calculated with the area method for a detector-wise response by performing an inhomogeneous with external source calculation for both the prompt and total flux to get the reactivity from Equation 18. The simulated result for case I3 shows good agreement with the references for the fiber detector and detector 15X. For the 10U detector the simulation result deviates from the average references result by 0.3β for ERANOS and 0.4β for PARTISN. In the case I5 the results show a good agreement with the references, but the PARTISN simulation for the fiber detector leads to a deviation of 0.8β .

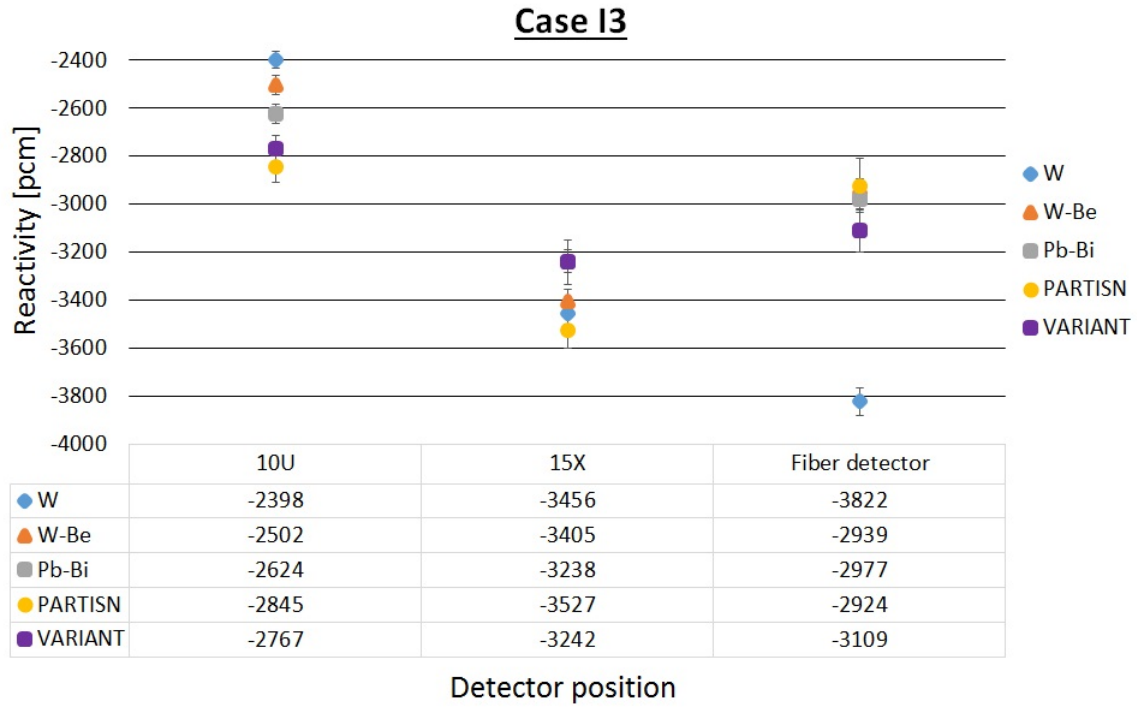


Figure 17: Result case I3.

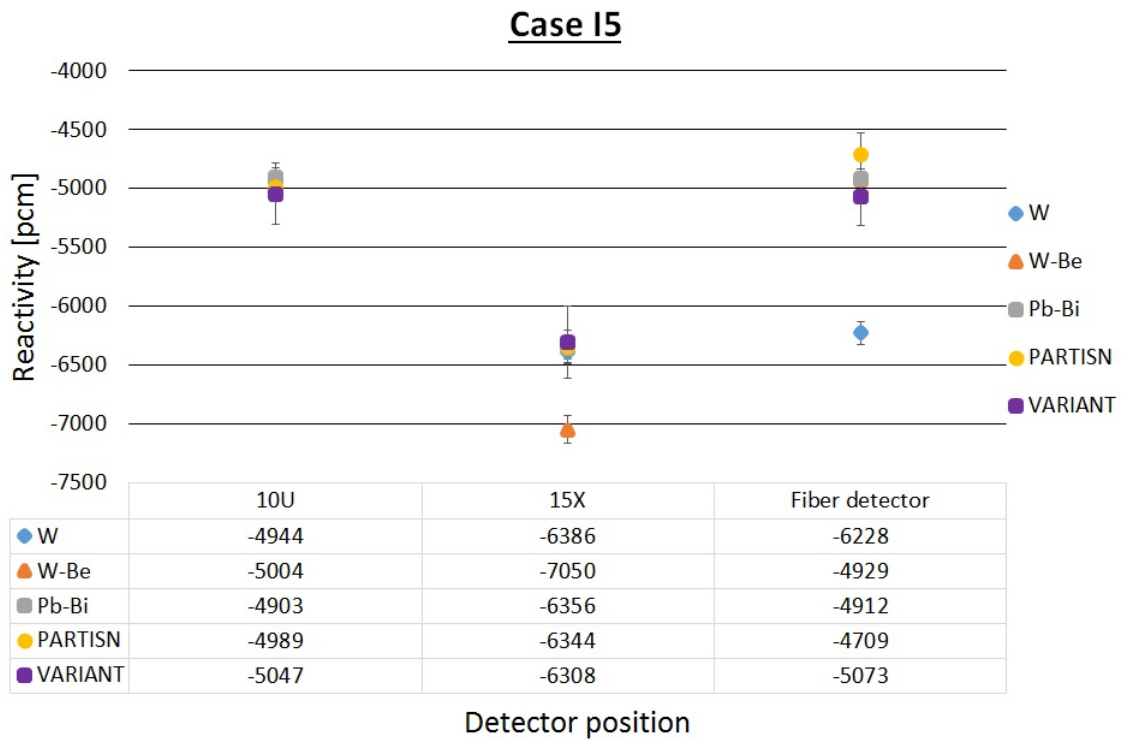


Figure 18: Result case I5.

5 Transient Analysis of Kinetics Experiments

As the static cases presented in Section 4.2, the transient calculations are performed in a 3D (XYZ) symmetry for the two core configurations, case I3 and case I5. The cross-sections are generated according to the methodology discussed in Section 3. The transient analyses have been performed with KIN3D/VARIANT and KIN3D/PARTISN codes according to the process scheme described in Section 2.2.5, by employing the quasistatic kinetic method that is mentioned in Section 2.1. To save computational time, 20 energy groups were used. The division from 40 to 20 energy groups does not deviate considerable (see Figure 19 for the direct flux and Figure 20 for the adjoint flux).

In the KUCA experiments, three different targets were used, namely *W*, *W-Be* and *Pb-Bi*. The reaction rates of the targets to core position were measured by an indium wire positioned in the core as presented in Figure 21. The deuterium-tritium source used in the simulation is compared with the experimental source Figure 22, where the normalized shapes are in agreement.

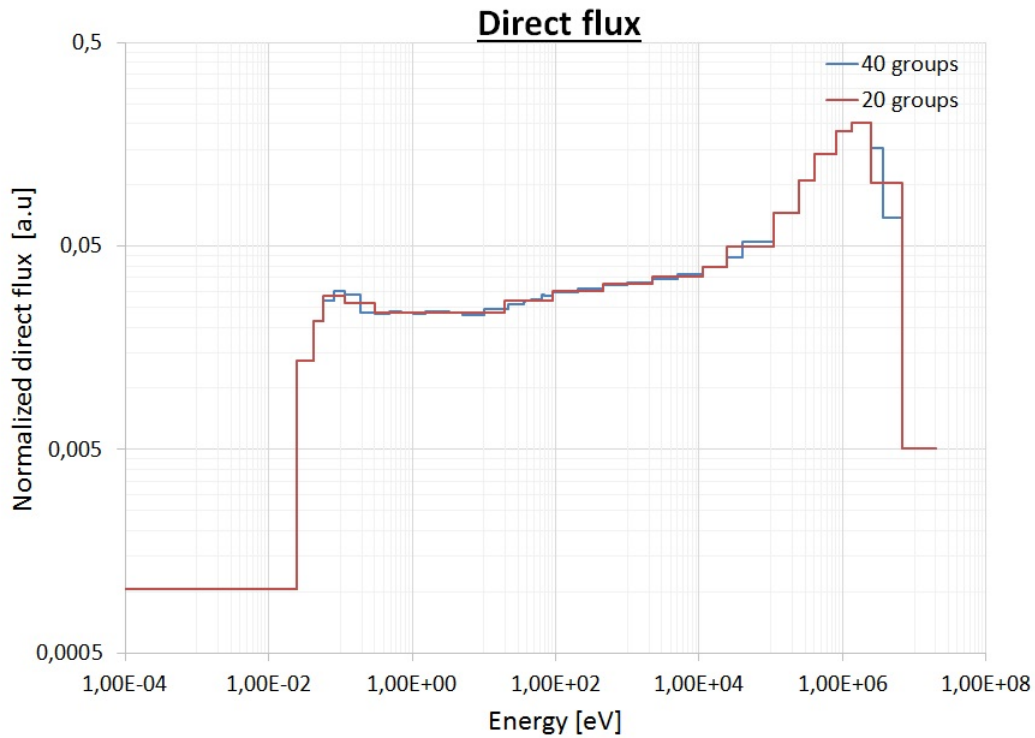


Figure 19: Direct flux.

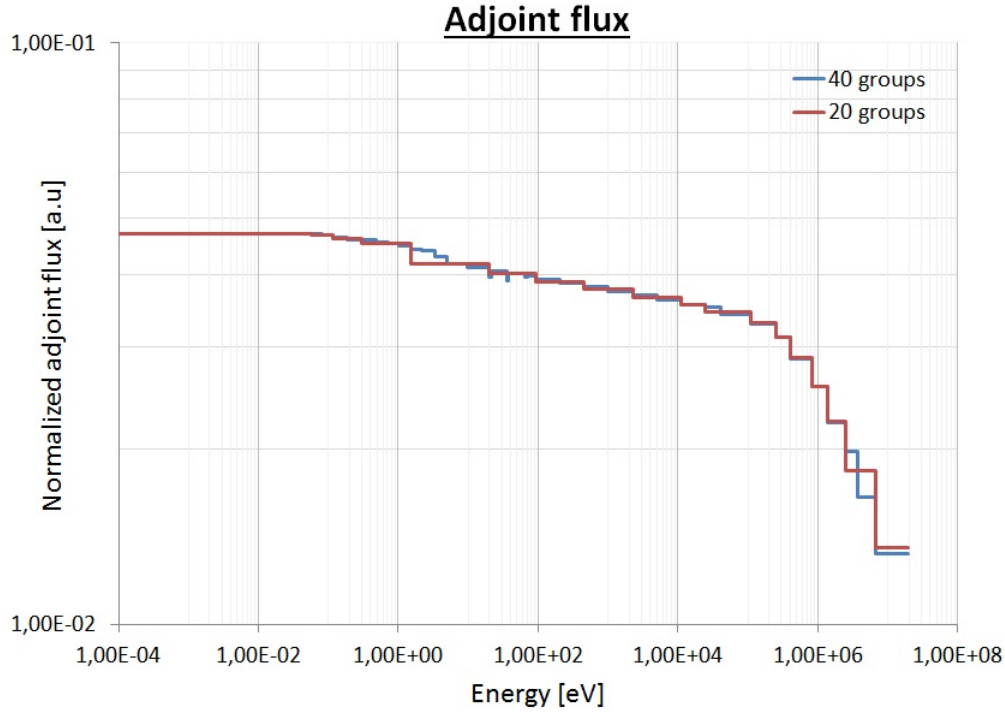


Figure 20: Adjoint flux.

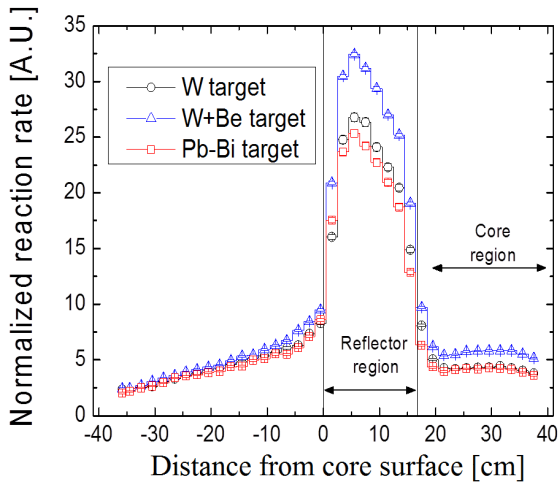


Figure 21: Reaction rates for the three targets used during the experiment.

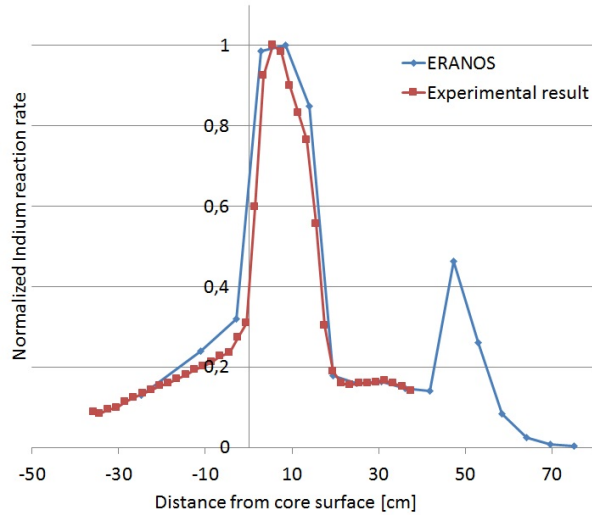


Figure 22: Normalized reaction rate for simulated deuterium-tritium source and one of the targets from the experiment.

The response of the KUCA reactor, to a pulsed neutron source is evaluated. In the simulations performed the source was modelled as a neutron pulse at the beginning of the transient, at the position of the target. The source used was a D-T source with a pulse length of 80 ns. The system response consists of a peak because of the prompt neutrons. The peak quickly dies out since the core is subcritical. The neutron flux decays to the level provided by the delayed neutrons which have larger time constants in comparison to the source pulse and the prompt neutron generation time.

The measurements performed at KUCA start at time $5E-5$ seconds, and therefore the results from the simulations are taken from this time. This means that the pulse in the beginning of the transient is excluded from the result since it occurs before this time, and only the system response to the pulse is considered. The results are then normalized to the maximum neutron flux during the measurement. Since the curve is normalized to the maximum neutron flux, the buildup of precursors must be the same as in the experiment. The simulated reactor has eight delayed families with different decay constants which are all larger than the prompt neutron decay constant of $\sim 0.1 \mu s$. The prompt neutrons will therefore only give contribution during the pulse, while the delayed neutrons will contribute during the pulse and several seconds afterwards. To get the correct buildup of precursors in the system and to make the result comparable with the experiment one restart calculations was performed [22]. So, the restart calculation is performed to be sure that the space-wise concentration of the precursors of the delayed neutrons is in equilibrium.

The mean neutron generation time for KIN3D/VARIANT for case I3 and case I5 is found in Figure 23. The mean neutron generation time between the two systems differ since the two systems have different subcriticality, case I5 reaches a deeper subcritical compared to case I3. Because of the different subcriticality, case I5 reaches the initial mean neutron generation time later then case I3. The kinetic parameters in Table 8 are valid for the transient as well.

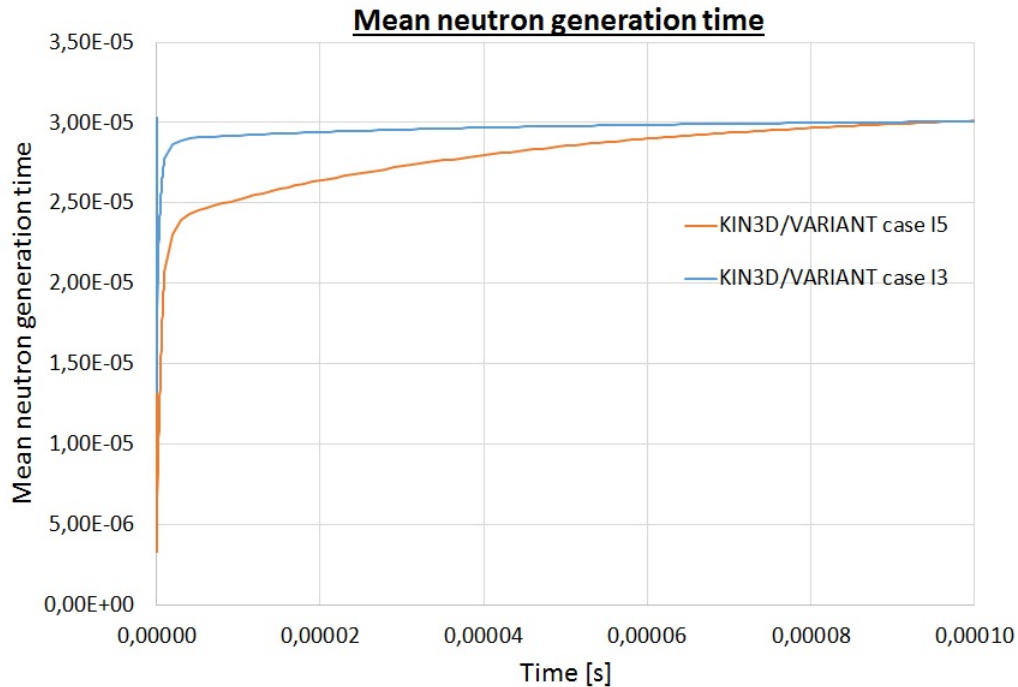


Figure 23: Mean neutron generation time.

Three detectors are available as described in Figure 6. In particular, the detectors 10U and 15 X were placed in the reflector and the optical fiber detector in the fuel. The results from the experiment and both transport solvers are plotted for case I3 for detector 10U is in Figure 24. The KIN3D/VARIANT are also plotted with a restart calculation, for which the effect is evident. Both transport solvers follow the correct shape of the slope, and reproduce the system behaviour very well. In Figure 25 results for detector 15X for case I3 are shown, and also here both KIN3D/VARIANT and KIN3D/PARTISN reproduce the experiment well with the restart calculation. The last detector for case I3 is the fiber detector in the fuel region. The results are found in Figure 26, and also here both transport solvers are able to recreate the experimental data. The spatial effects for case I3 are captured with the simulations for all detectors and follow the shape of the curve as expected.

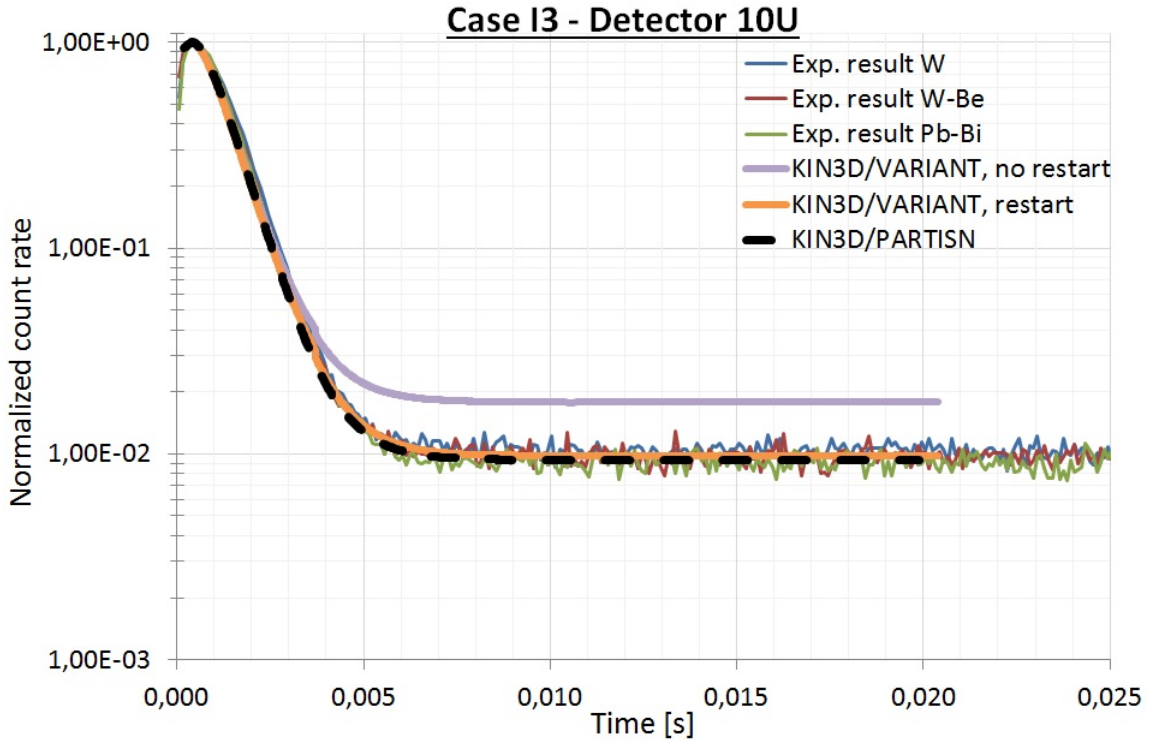


Figure 24: Comparison between simulations and measurements from detector 10U, in case I3.

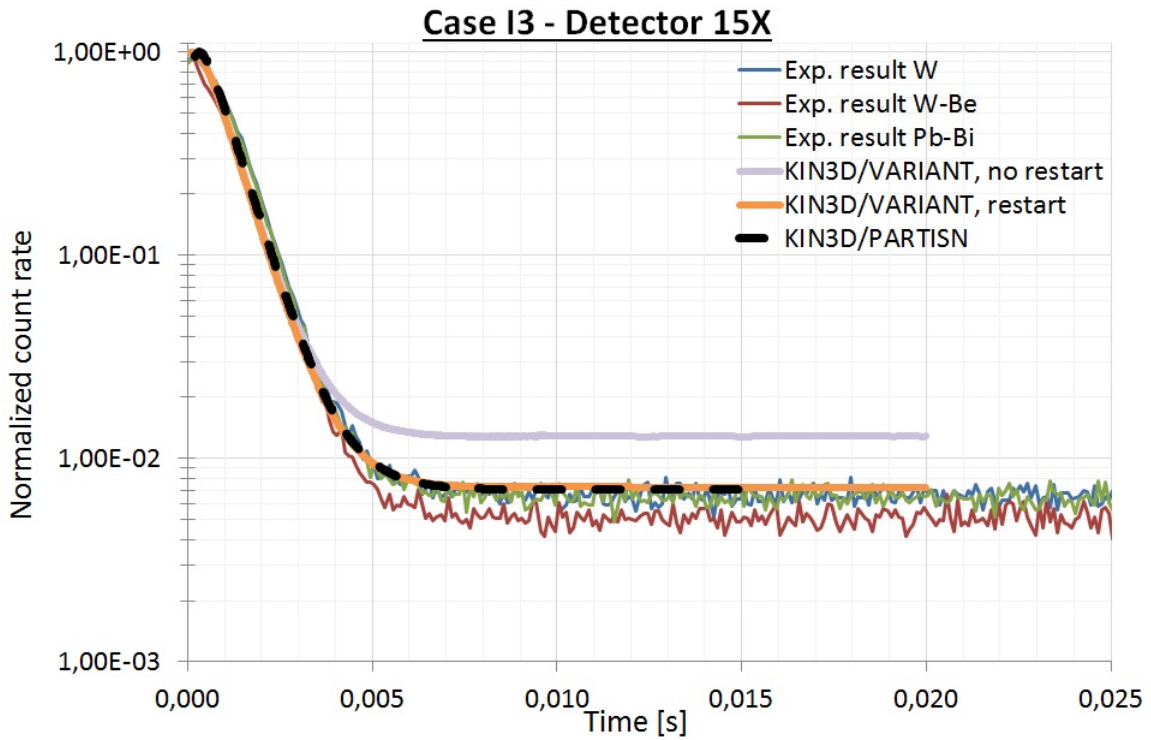


Figure 25: Comparison between simulations and measurements from detector 15X, in case I3.

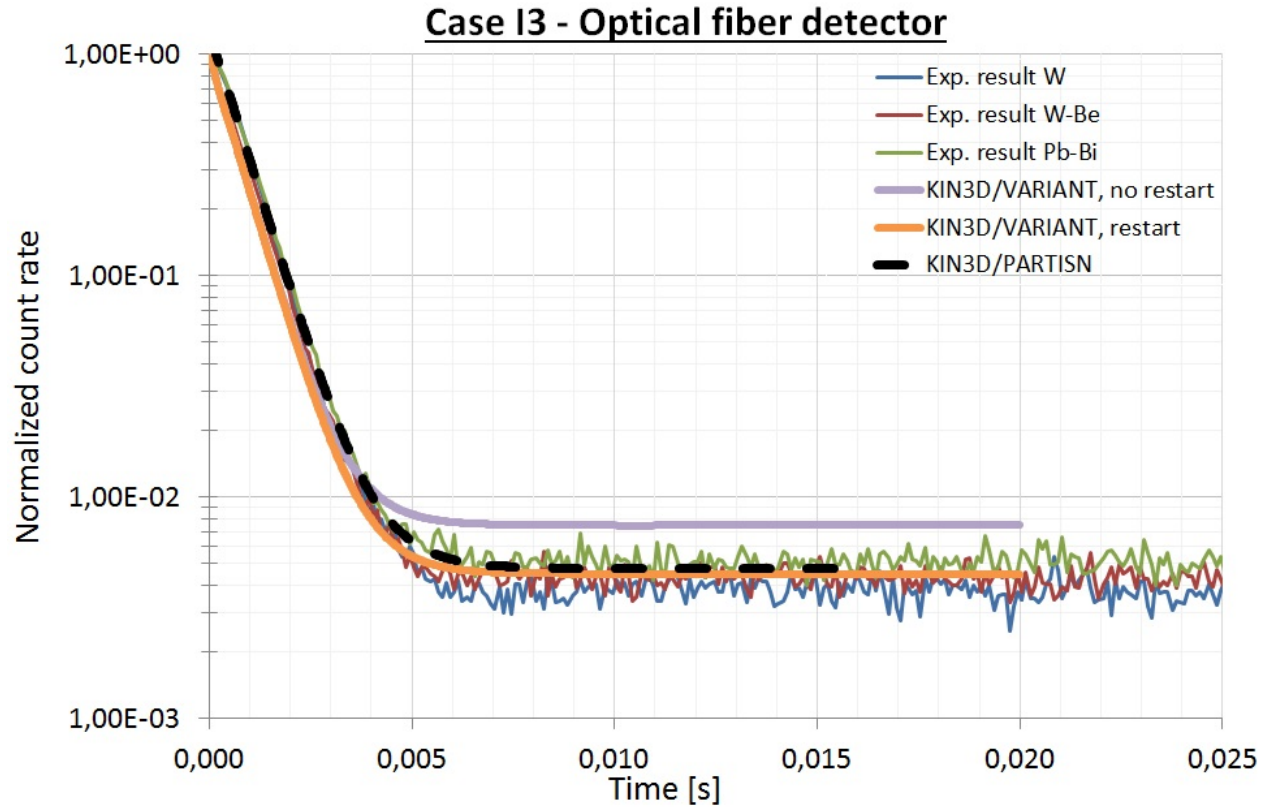


Figure 26: Comparison between simulations and measurements from the optical fiber detector, in case I3.

For Case I5 the difference between the simulation with and without restart is not as large as in case I3 since this system is more subcritical and therefore less sensitive to perturbations. KIN3D/PARTISN reproduces well the experimental measurements from detector 10U for case I5, while KIN3D/VARIANT overestimates the average level even for the simulation without restart. The comparisons are summarized in Figure 27.

The simulated results for 15X follow the experimental data for both the KIN3D/VARIANT code KIN3D/PARTISN, see Figure 28. Also, the measurements of the fiber detector could be predicted with both codes options, see Figure 29. For this case, the KIN3D/VARIANT calculation follows the experimental Pb-Bi result while KIN3D/PARTISN follows the experimental W result better. However, both simulations slightly differ from the average level. The two codes used for the transient analyses are based on different simulation strategies, so discrepancies are expected. The overall results show good agreement with the experiment and the spatial effect could be reproduced.

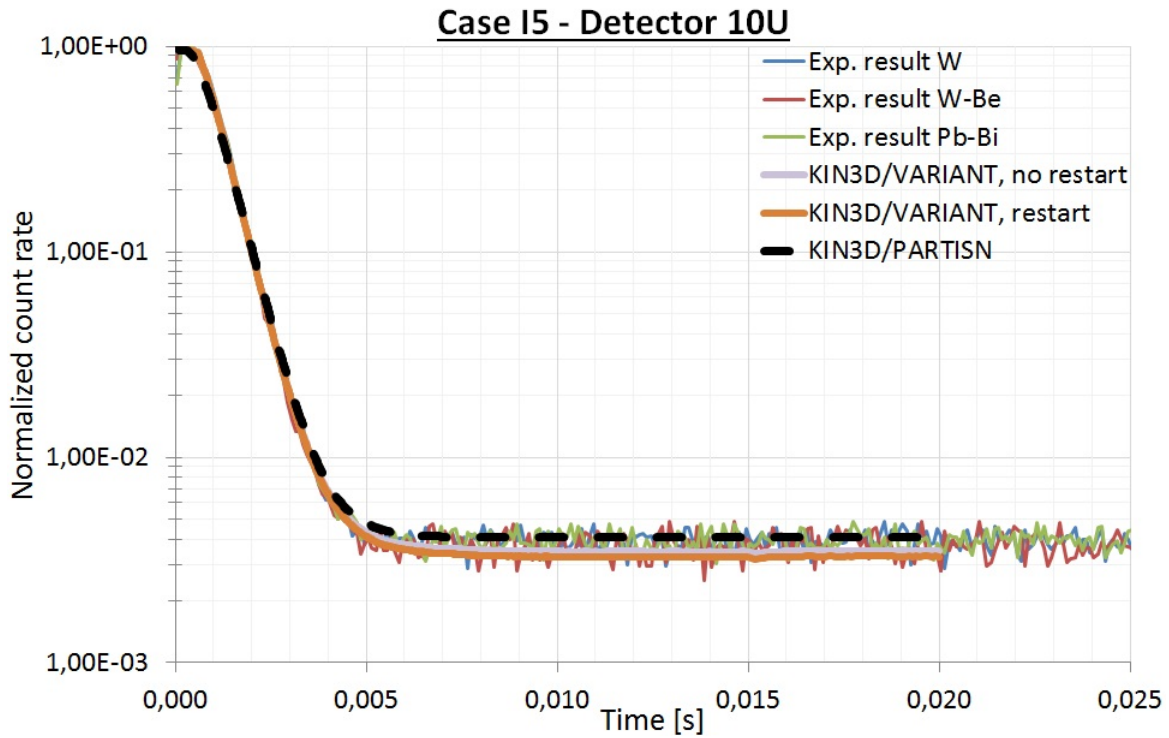


Figure 27: Comparison between simulations and measurements from detector 10U, in case I5.

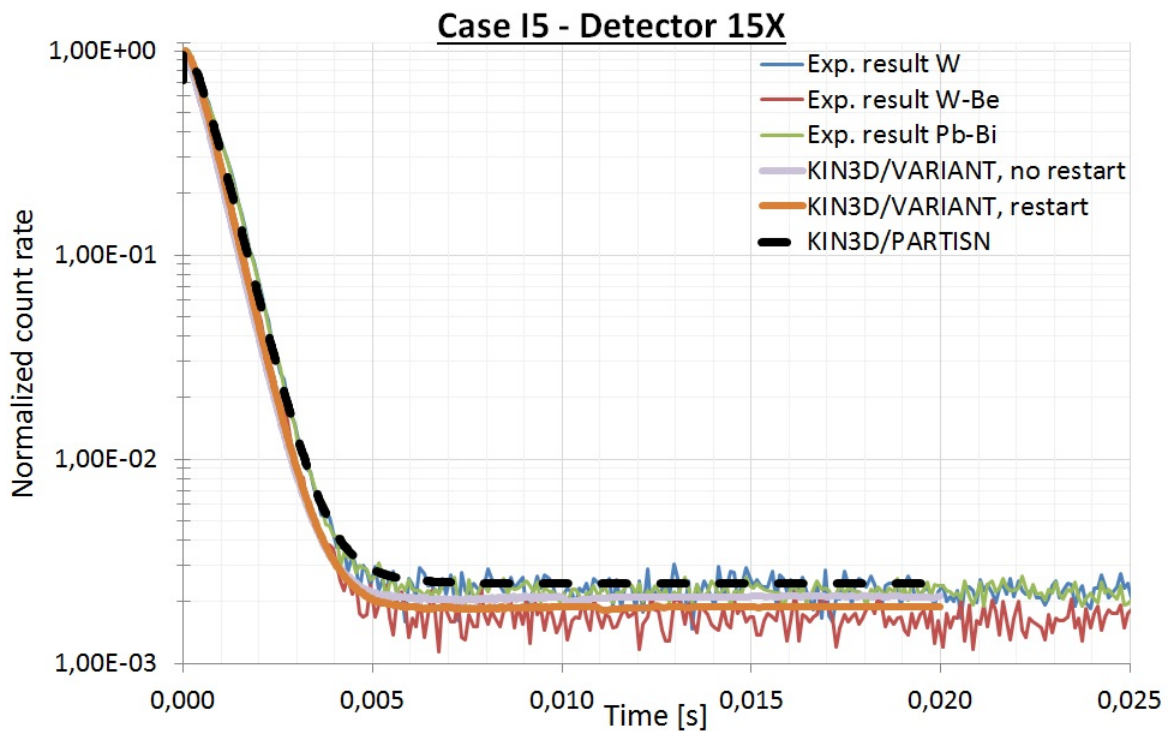


Figure 28: Comparison between simulations and measurements from detector 15X, in case I5.

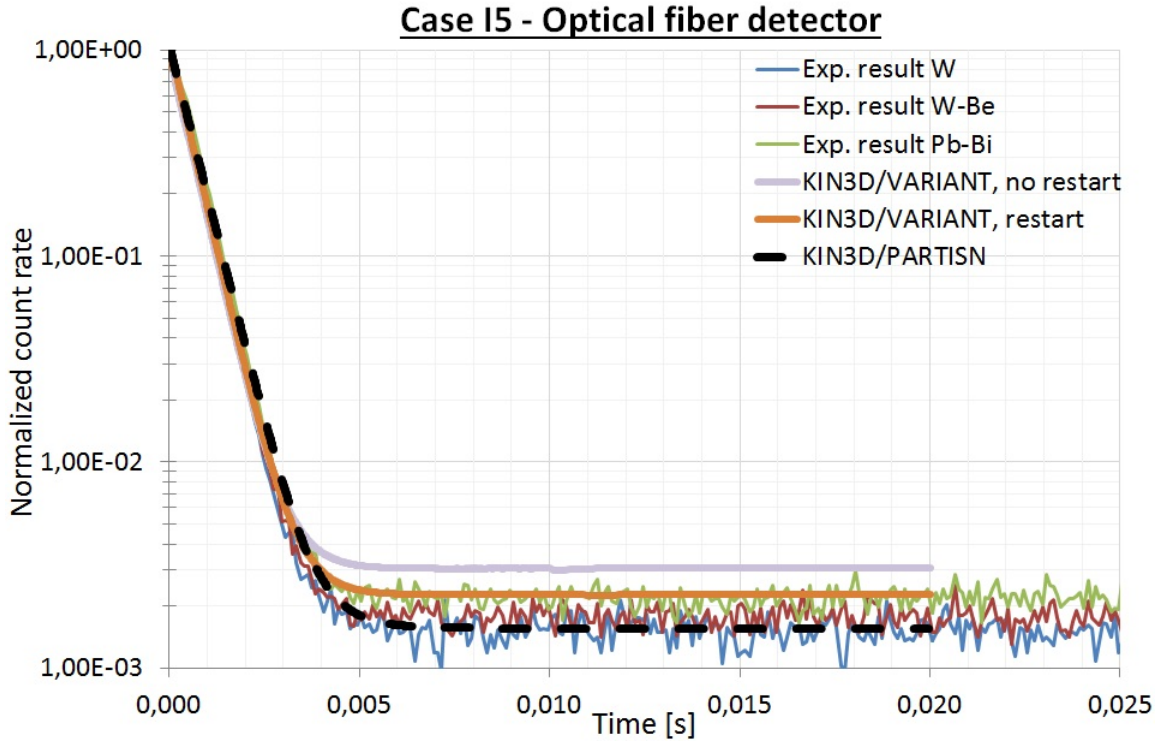


Figure 29: Comparison between simulations and measurements from the optical fiber detector, in case I5.

6 Conclusion

Computer simulations provide a significant safety barrier for nuclear technology, and the work of assessing codes against experimental data is of great importance. The nuclear codes need to be reliable and accurate, which is improved by studying kinetics experiments and model them with kinetics codes. With this in mind, the analysis of both static and transient calculations are essential for improving the deterministic codes.

ADS is one option under investigation, for the treatment of long-lived radioactive materials produced in nowadays commercial reactors. In ADS the reactivity level has to be continuously monitored since the system mostly consists of prompt neutrons due to the fuel with a high mass fraction of minor actinides. Therefore, computational capabilities should be developed and their accuracy and reliability require to be assessed against proper experiments.

ADS systems have as mentioned strong perturbation caused by the external source, which have been analyzed with a detector-wise response to such a source. This thesis performed at KIT is in the calculation benchmark launched by the Kyoto University Research Reactor Institute (KURRI). The kinetics experimental data which has been analyzes is from the Phase-I kinetics experiments performed at Kyoto University Critical Assembly (KUCA). This is done in the frame of the IAEA Collaborative work on ‘Accelerator Driven Systems (ADS) and Use of Low-Enriched Uranium (LEU) in ADS’.

The purpose of the thesis was to reproduce the experiments performed at KUCA for case I3 and case I5. Cross-sections for the KUCA reactor were generated by making use of the lattice code ECCO. In this part of the work, a methodology was applied to adjust the boron content of the control rods and optimize cross-sections in a systematic manner. The procedure was proven to provide good results with respect to the KUCA reference values and the Monte Carlo simulations. Once the cross-sections for KUCA had been created, they were used in a 3D (XYZ) model built with European Reactor ANalysis Optimized System (ERANOS). The static analysis was then performed with both Variational Anisotropic Neutron Transport (VARIANT) and PARallel TIme-dependent SN code (PARTISN). Static calculations with VARIANT and PARTISN give good agreement with the experimental data, in terms of both k-effective and kinetic parameters. Furthermore, pulsed experiments were investigated for the purpose of reactivity estimation and for transient analyses. As regards reactivity estimation with pulse experiments, the area method was applied. The results based on the VARIANT and PARTISN simulations and on the experimental measurements from the three detectors available in KUCA, are found to be consistent.

The time-dependent calculations were also analyzed in respect of a detector-wise response to an external neutron source. In the aim of analysing the transient experimental results KIN3D/VARIANT and KIN3D/PARTISN were employed. The improved-quasistatic approach was used and the result show that the codes could reproduce the experimental results. The deterministic codes could reasonable well reproduce the experimental result and the spatial effect of the reactor in both the static and transient cases.

References

- [1] *Outline History of Nuclear Energy*. URL: <http://www.world-nuclear.org/information-library/current-and-future-generation/outline-history-of-nuclear-energy.aspx> (visited on 11/17/2016).
- [2] A. Nordlund. *Introduction to nuclear reactors*. 2015.
- [3] European nuclear society. *Nuclear power plants, world-wide*. URL: <https://www.euronuclear.org/info/encyclopedia/n/nuclear-power-plant-world-wide.htm> (visited on 02/05/2017).
- [4] World Nuclear Organisation. *Plans For New Reactors Worldwide*. URL: <http://www.world-nuclear.org/information-library/current-and-future-generation/plans-for-new-reactors-worldwide.aspx> (visited on 02/05/2017).
- [5] Nuclear Energy Institute. *On-Site Storage of Nuclear Waste*. URL: <https://www.nei.org/Knowledge-Center/Nuclear-Statistics/On-Site-Storage-of-Nuclear-Waste> (visited on 02/05/2017).
- [6] World Nuclear Organisation. *What are nuclear wastes and how are they managed?* URL: <http://www.world-nuclear.org/nuclear-basics/what-are-nuclear-wastes.aspx> (visited on 02/05/2017).
- [7] World Nuclear Association. *Radioactive Waste Management*. URL: <http://www.world-nuclear.org/information-library/nuclear-fuel-cycle/nuclear-wastes/radioactive-waste-management.aspx> (visited on 05/25/2017).
- [8] *A European Roadmap for Developing Accelerator Driven Systems (ADS) for Nuclear Waste Incineration*. The European Technical Working Group on ADS. Apr. 2001.
- [9] H. Abderrahimh, J. Galambosd, Y. Gohara, (...), R. Sheffielde, and M. Todosowb. “Accelerator and Target Technology for Accelerator Driven Transmutation and Energy Production”. In: *FERMILAB-FN-0907-DI* LA-UR-10-06754 (Sept. 17, 2010).
- [10] A. Rineiski. *KIN3D: A space-time kinetics and perturbation theory module for TGV2*. CEA/Cadarache. July 1, 1999.
- [11] F. Gabrielli, A. Rineiski, W. Maschek, and M. Marchetti. “Reactor Transient Analyses with KIN3D/VARIANT”. In: *International Conference on Mathematics and Computational Methods Applied to Nuclear Science & Engineering (M&C 2013), Sun Valley, Idaho, USA,,* May 5-9 (2013).
- [12] G. Rimpault. *Algorithmic features of the ECCO cell code for treating heterogeneous fast reactor assemblies*. Portland, Oregon, USA, May 1995. ISBN: 0-89448-198-3.
- [13] J. Y. Doriath et al. “ERANOS1: The Advanced European System of Codes for Reactor Physics Analysis”. In: *Proc. Int. Conf. on Mathematical Methods and Supercomputing in Nuclear Applications* (1993).
- [14] C. B. Carrico, E. E. Lewis, and G. Palmiotti. “Three-dimensional Variational Nodal Transport Methods for Cartesian, Triangular and Hexagonal Criticality Calculations”. In: *Nuclear Science and Engineering* (1992), pp. 111–168.
- [15] I. Dilber and E. E. Lewis. “Variational Nodal Methods for Neutron Transport”. In: *Nuclear Science and Engineering* (1985), pp. 91–132.
- [16] *PARTISN 5.97, 1-D, 2-D, 3-D Time-Dependent, Multigroup Deterministic Parallel Neutral Particle Transport Code*. OECD/NEA Data Bank. 2009.
- [17] C. Pyeon. *Neutronics on Solid Pb-Bi in Accelerator-Driven System with 100 MeV Protons at Kyoto University Critical Assembly*. Research Reactor Institute, Kyoto University, Japan, Aug. 30, 2016.
- [18] F. Gabrielli, A. Rineiski, M. Marchetti, M. Massone, and V. Kriventsev. “Study of the effect of heterogeneity of the control rods on the Phénix reactor”. In: *PHYSOR 2014 – The Role of Reactor Physics Toward a Sustainable Future, Kyoto, Japan,* Sept 28 – Oct 3 (2014).
- [19] Nils Göran Sjöstrand. “Measurements on a subcritical reactor using a pulsed neutron source”. In: *Arkiv Fysik* 11.13 (Apr. 11, 1956).

- [20] N. Marie, G. Lehaut, J.L. Lecouey, (...), H.E. Thyébault, and D. Villamarin. “Reactivity monitoring using the area method for the subcritical VENUS-F core within the framework of the FREYA Project”. In: *International Workshop on Technology and Components of Accelerator Driven Systems (TCADS) OECD Nuclear Energy Agency, Nantes, France* (June 5, 2013).
- [21] G. I. Bell and S. Glasstone. *Nuclear Reactor Theory*. New York, USA: Van Nostrand Reinhold Company, 1970.
- [22] A. Talamo, Y. Gohar, C. Rabiti, G. Aliberti, (...), C. Routkovskaya, and I. Serafimovich. “Pulse superimposition calculational methodology for estimating the subcriticality level of nuclear fuel assemblies”. In: *Nuclear instrument and methods in physics research A* 606.3 (May 3, 2009), pp. 661–668.